

University of Richmond

UR Scholarship Repository

Honors Theses

Student Research

2020

Synthesis, Characterization, and Reactivity of Palladium Proazaphosphatrane Complexes

Adrian D. Matthews
University of Richmond

Follow this and additional works at: <https://scholarship.richmond.edu/honors-theses>

 Part of the [Chemistry Commons](#)

Recommended Citation

Matthews, Adrian D., "Synthesis, Characterization, and Reactivity of Palladium Proazaphosphatrane Complexes" (2020). *Honors Theses*. 1500.
<https://scholarship.richmond.edu/honors-theses/1500>

This Thesis is brought to you for free and open access by the Student Research at UR Scholarship Repository. It has been accepted for inclusion in Honors Theses by an authorized administrator of UR Scholarship Repository. For more information, please contact scholarshiprepository@richmond.edu.

Synthesis, Characterization, and Reactivity of Palladium Proazaphosphatrane Complexes

by

Adrian D. Matthews

Honors Thesis

Submitted to:

Chemistry Department
University of Richmond
Richmond, VA 23173

May 1, 2020

Advisor: Dr. Miles Johnson

Abstract

Palladium-catalyzed cross-coupling reactions provide an efficient pathway to a wide variety of otherwise inaccessible compounds. In this study, the synthesis and reactivity of novel palladium proazaphosphatranes complexes that are believed to be intermediates in C–N cross-coupling reactions are described. Both the fundamental reactivity of these complexes and elementary steps involved in a catalytic process are demonstrated. The catalytic viability of palladium proazaphosphatranes complexes is shown through stoichiometric and catalytic cross-coupling reactions. Our findings support the long-standing hypothesis that proazaphosphatranes are conformationally flexible ligands that stabilize a number of catalytic intermediates.

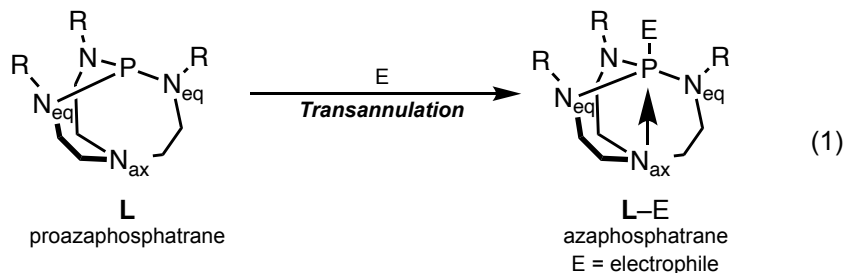
Introduction

Cross-coupling reactions have emerged as a powerful synthetic tool in the last few decades. Through the use of a metal catalyst, these reactions enable the formation of a new bond between sterically hindered or unreactive coupling partners. Relative to stoichiometric reactions, the use of a metal catalyst can prevent chemical waste, reduce overall energy costs, and enable smarter synthetic design, involving fewer steps and producing desirable and elusive products.¹ While a number of transition metals have been used in cross-coupling, palladium catalysts have proven to be particularly useful in the fine chemical, agrochemical, and pharmaceutical industries due to their ability to facilitate the formation of new carbon–carbon (C–C) and carbon–nitrogen (C–N) bonds.² Well-studied, named palladium cross-coupling reactions such as Heck, Negishi, Suzuki, and Buchwald-Hartwig amination show particular relevance in pharmaceutical synthesis, where close to two-thirds of C–C bond formations are mediated by palladium complexes.³

While improvements of commonly invoked cross-coupling reactions focused initially on investigations of metals and coupling partners, in recent years, attention has shifted to an examination of ligand properties as a means to control catalytic reactivity.⁴ Studies of electronic properties of ligands have demonstrated that the use of electron-rich phosphine ligands in palladium complexes increase the rate of oxidative addition. Electron-rich ligands also coordinate more tightly to the metal center and disfavor the formation of palladium black, extending the lifetime of these catalysts. Conversely, sterically demanding phosphine ligands facilitate reductive elimination by crowding other ligands and favoring monophosphine or monocarbene palladium species.⁵ Coupling of sterically hindered substrates, however, requires that a ligand be both small enough to accommodate bulky substrates and large enough to promote reductive elimination. Ligands with some degree of steric flexibility therefore greatly expand the number of products formed via cross-coupling reactions.⁵

Proazaphosphatranes are a class of particularly versatile flexible ligands frequently used in organometallic complexes to facilitate the cross-coupling of sterically hindered partners. Proazaphosphatranes are strong, aminophosphine bases with a cage-like structure.⁶ Measurements of cone angles and Tolman electronic parameters have placed proazaphosphatranes among the bulkiest and most electron-donating phosphine ligands, making them of particular interest as ligands in cross-coupling reactions.⁷ In addition, proazaphosphatranes show considerable flexibility dependent on the electronic and steric crowding from other reactive ligands. When

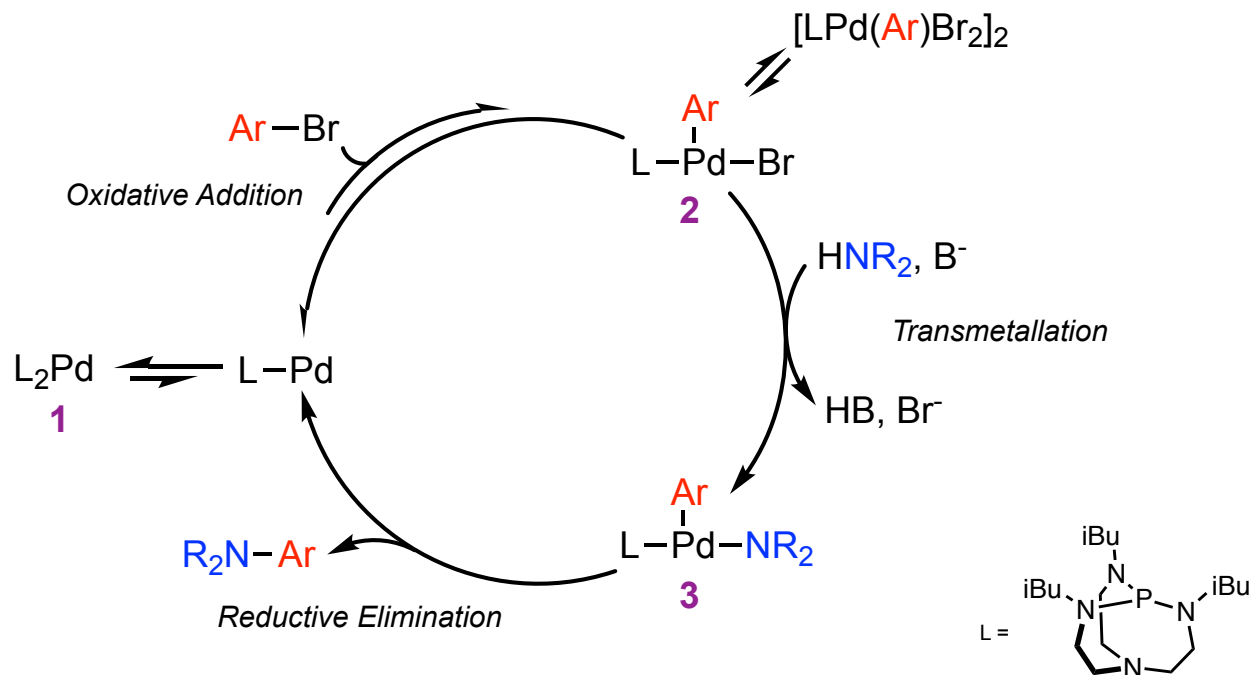
bound to an electrophile, proazaphosphatranes undergo a dramatic structural change induced by transannulation, the intramolecular interaction between the axial nitrogen and phosphorous, to form an azaphosphatrane (eq 1).



The versatility of proazaphosphatranes as ligands in cross-coupling reactions is largely predicated on this transannular interaction, which promotes key catalytic steps. It is believed that steric bulk at the equatorial nitrogen facilitates reductive elimination, electron donation due to transannulation promotes oxidative addition, and transannulation increases with electron deficiency at the metal center.^{8,9} As a testament to their versatility, proazaphosphatranes have been widely employed as ligands in palladium catalyzed cross-coupling reactions, including Suzuki,¹⁰ Buchwald-Hartwig,⁸ and Stille,¹¹ and as ligands in a number of organometallic complexes.

Despite the invocation of proazaphosphatranes as ligands in palladium-catalyzed cross-coupling reactions, palladium proazaphosphatrane complexes were unreported prior to this work.¹² Gaining insight into the coordination chemistry of palladium proazaphosphatrane complexes both provides support for the long-standing hypothesis that the ligand's variable transannulation stabilizes catalytic intermediates as well as provides a framework for future catalyst design. In this study, palladium proazaphosphatrane complexes for application in Buchwald-Hartwig amination are prepared and studied. The hypothesized mechanism and intermediates involved in Buchwald-Hartwig amination in terms of palladium-proazaphosphatrane complexes are shown in Scheme 1. The most prolifically employed proazaphosphatrane, 2,8,9-triisobutyl-2,5,8,9-tetraaza-1-phosphabicyclo[3.3.3]undecane (**L**) was chosen as the ligand of interest. Buchwald-Hartwig amination was chosen as a model system both because its mechanism has been thoroughly investigated and because **L** is known to facilitate this reaction.^{9,13}

Scheme 1. Mechanism for C–N Cross-Coupling



Results and Discussion

A palladium bisproazaphosphatrane complex (**1**) was prepared by treating Pd_2dba_3 with 4.5 equiv. of **L** (eq 2). Both the solvent and palladium source mimic those frequently invoked in other reported catalytic reactions.¹⁴ Crystals of the resulting complex were grown, demonstrating the solid-state structure of complex **1** as linear following X-ray crystallographic analysis (Figure 1).

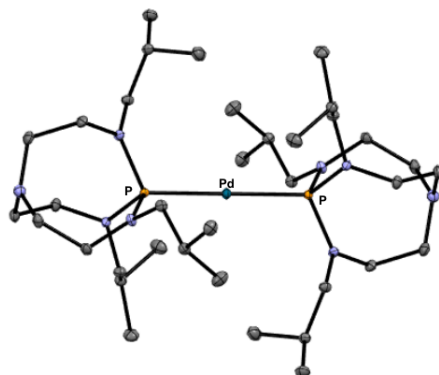
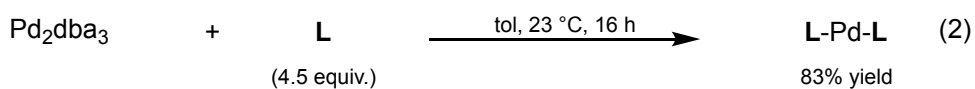


Figure 1. ORTEP diagram of complex **1**. Ellipsoids are shown at 50% probability. Hydrogens are excluded for clarity.

Treatment of complex **1** with a variety of aryl halides to form palladium oxidative addition complexes was unsuccessful, potentially due to the high energy barrier associated with dissociating **L** from the palladium bisproazaphosphatrane complex. The inability to interconvert between complex **1** and complex **2** precluded the possibility of conducting thermodynamic studies. Instead, the treatment of $\text{Pd}(\text{COD})(\text{CH}_2\text{TMS})_2$ with aryl bromides and **L** in an orthogonal, low-temperature approach yielded palladium(II) oxidative addition complexes in moderate yield (eq 3). Half-life studies showed that the stability of these palladium oxidative addition complexes in solution tracked with the relative electron-donating properties of the aryl ligands, with the half-life of electron-rich complex **2d** being only minutes but electron-poor complexes **2a** and **2b** remaining stable in solution over several days (Table 1). The complexes decomposed in solution to form mixtures containing complex **1**, palladium black, and biaryls (see Supporting Information). X-ray crystallography was used to characterize the more stable complexes **2a** and **2b** as dimers, a result consistent with the solid-state forms of other previously published similar palladium phosphine complexes (Figure 2).^{15,16}

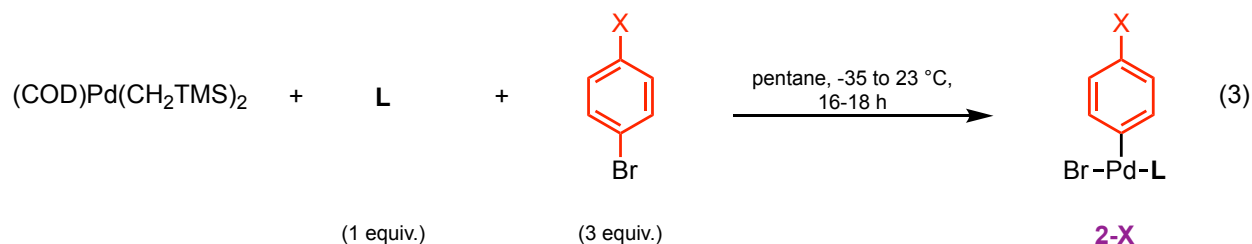


Table 1. Half-lives of Palladium Oxidative Addition Complexes

	X	Yield	t_{1/2}
2a	CN	80%	5-6 d
2b	CF ₃	66%	5-6 d
2c	H	72%	14-16 hr
2d	OMe	56%	15-30 min

t_{1/2} indicates half life of compound

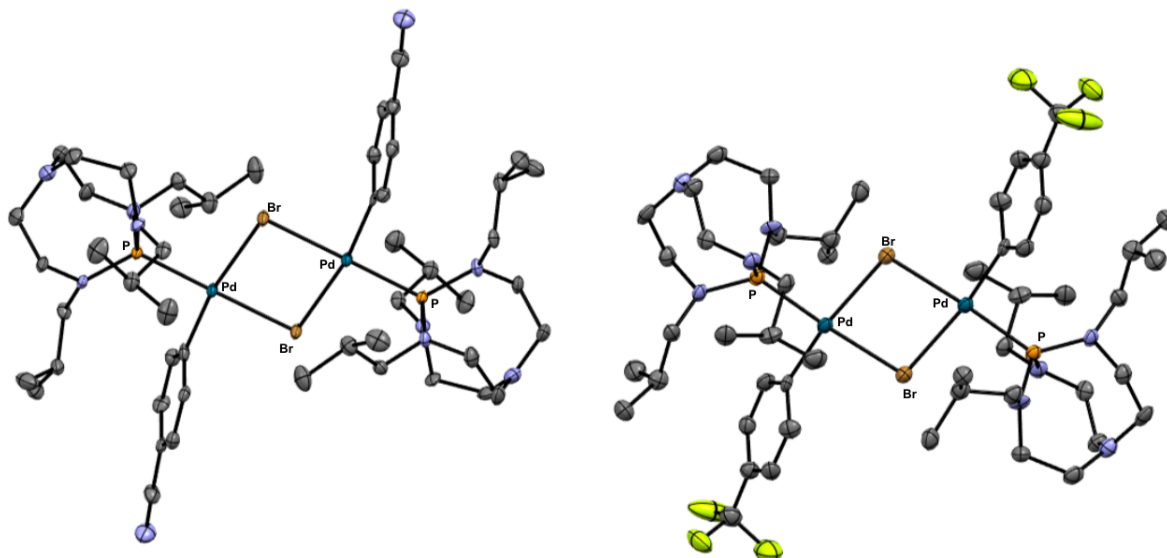
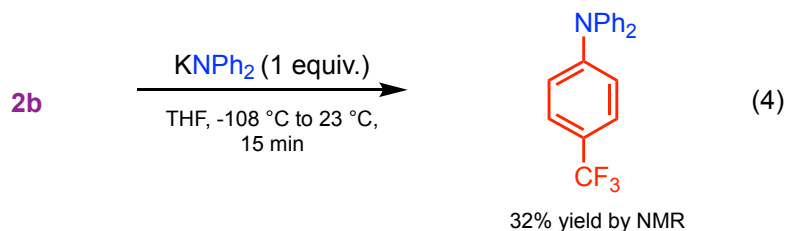


Figure 2. ORTEP diagram of complex **2a** (left) and **2b** (right). Ellipsoids are shown at 50% probability. Hydrogens and solvent molecules are excluded for clarity.

The remaining putative intermediate in the Buchwald-Hartwig catalytic system, a palladium amido complex, was generated so that its reactive properties could be similarly examined. A first attempt to isolate a palladium proazaphosphatrane amido complex, via the treatment of complex **2b** with KNPh_2 at low temperature, instead formed the corresponding triarylamine and palladium black (eq 4). While the reaction mixture was initially a dark red, within several minutes it faded to black. The formation of triarylamine is consistent with findings that three-coordinate palladium amido complexes readily undergo reductive elimination even at low temperatures. The presence of an electron donating aryl group in the oxidative addition complex, though, has been shown to prevent reductive elimination and stabilize the amido intermediate.¹⁷ Treatment of electron-rich complex **2d** with electron-poor amide $\text{KN}[3,5-(\text{CF}_3)_2\text{C}_6\text{H}_3]_2$ yielded complex **3** (eq 5), which was also characterized crystallographically (Figure 3).



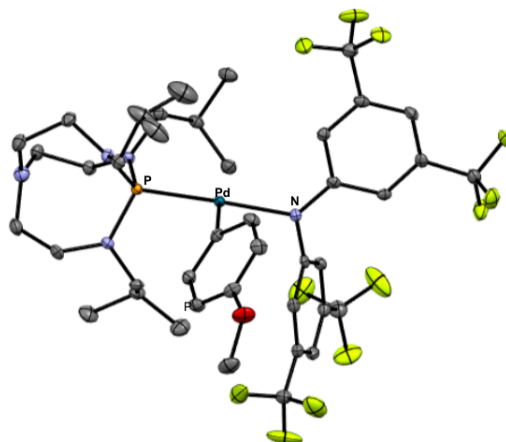
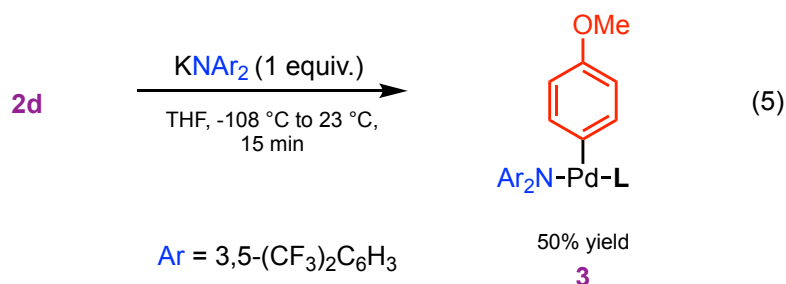
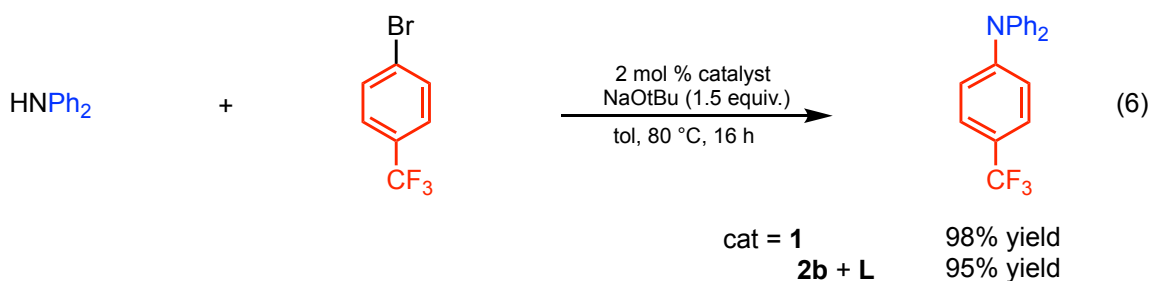


Figure 3. ORTEP diagram of complex **3**. Ellipsoids are shown at 50% probability. Hydrogens are excluded for clarity.

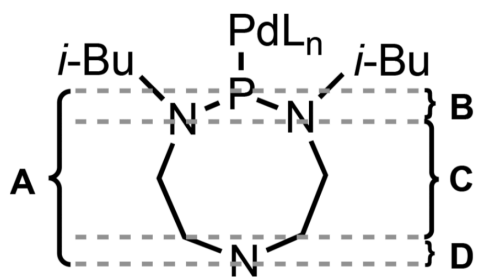
The catalytic viability of complexes **1**, **2b**, and **3** in Buchwald-Hartwig amination were examined in stoichiometric and catalytic reactions. Under literature conditions,⁹ complexes **1** and **2b** were successful catalysts in the cross-coupling of diphenyl amine with 4-bromobenzene (eq 6), demonstrating their potential industrial relevance. Complex **3** did not demonstrate any catalytic viability, consistent with its inability to undergo reductive elimination stoichiometrically (see eq 5), but it remains a unique example of such a molecule and provides insight into the broader catalytic system by enabling an examination of variable transannulation in proazaphosphatranine systems.



To address the degree to which proazaphosphatranine ligands demonstrate variation in transannulation across metal complexes, the transannular distance was studied in each of the

prepared palladium proazaphosphatrane complexes (Table 2). Complex **1** displayed the greatest transannular distance (3.482 Å), likely due to influence of the two highly electron-donating trans proazaphosphatrane ligands on the metal center. This distance is similar to that observed in nickel(0) complexes.⁷ The observed transannular distance was shorter for complexes **2a** and **2b** (3.260 Å and 3.265 Å, respectively) and shortest for complex **3**, in which the palladium center has only a single L-type ligand, a trend which supports the hypothesis that transannulation increases with increasing electron deficiency at the metal center. Examining the transannular distance in more detail reveals that the change in transannular distance is a function of shortening over distances B and D. These results represent the first study of transannulation in proazaphosphatranes set on a single metal and provide evidence for the long-standing hypothesis that the catalytic viability of proazaphosphatranes derives from their unique flexibility.

Table 2. Key Distances in Proazaphosphatrane L^a



	A (Å)	B (Å)	C (Å)	D (Å)
1	3.481(2)	0.714(1)	2.563(2)	0.205(2)
2a^b	3.260(6)	0.644(4)	2.515(5)	0.107(7)
2b	3.265(7)	0.628(4)	2.522(5)	0.122(8)
3	3.206(3)	0.628(4)	2.513(2)	0.067(3)

^aOne N(i-Bu)CH₂CH₂ group is excluded for clarity. ^bAverage of four distances in the unit cell.

Conclusions

In summary, this work represents the first synthesis of palladium proazaphosphatrane complexes. Catalytic and stoichiometric studies reveal reactivity consistent with their presence on the catalytic cycle and the potential industrial relevance of these complexes. Examination of the variable transannulation of proazaphosphatrane ligands on a single metal provide evidence that the ligands undergo significant conformational changes in response to the oxidation state of palladium and the coordination chemistry of the metal. Further synthetic studies undertaken by our group on haloazaphosphatranes have controlled for oxidation state and coordination chemistry of the electrophile and provided systematic evidence of the relationship between electron deficiency and transannulation and established a foundation for extensive computational studies of azaphosphatranes.¹⁸ The palladium proazaphosphatrane complexes isolated in this work may be

used as synthons for other proazaphosphatane catalysts, potentially expanding the applications of proazaphosphatane systems beyond C–N and C–C cross-coupling reactions.

Experimental Section

I. General Considerations. All reactions were carried out in a nitrogen-filled MBraun LABstar Pro glovebox unless otherwise noted. All glassware was oven-dried overnight at greater than 110 °C prior to use. All liquid aryl halides were passed through activated alumina and stored over 3 Å molecular sieves prior to use. 4-bromobenzotrifluoride (Aldrich), bromobenzene (Aldrich), 4-bromobenzonitrile (Oakwood), and 4-bromoanisole (Aldrich) were purchased from commercial sources. Anhydrous pentane was purchased from Aldrich and stored over 3 Å molecular sieves prior to use. All other solvents were collected from a Glass Contour Solvent Purification System, degassed, and stored over 3 Å molecular sieves. Anhydrous deuterobenzene (C_6D_6) was purchased from Aldrich and stored over 3 Å molecular sieves. $Pd_2(dba)_3$ (Aldrich), $(COD)Pd(CH_2TMS)_2$ (Strem), and 2,8,9-triisopropyl-2,5,8,9-tetraaza-1-phosphabicyclo[3,3,3]undecane (**L**, Aldrich) were used as received from their respective vendors. $KNPh_2$ ¹⁹ and $KN[3,5-CF_3(C_6H_3)]_2$ ²⁰ were prepared by literature procedures. 1,3,5-trimethoxybenzene was purified by sublimation. Authentic samples of biaryl compounds were prepared by literature methods.²¹ Chromatography was performed using SiliaFlash F60 silica.

Spectroscopy. 1H , $^{13}C\{^1H\}$, $^{19}F\{^1H\}$, and $^{31}P\{^1H\}$ spectra were collected on Bruker AV-300 and AV-500 NMR spectrometers at ambient temperature unless otherwise noted. 1H NMR chemical shifts (δ) are reported in parts per million (ppm) relative to the solvent (7.16 ppm for C_6D_5H). ^{13}C NMR spectra were referenced relative to the solvent signal (128.06 ppm for C_6D_6). $^{31}P\{^1H\}$ and $^{19}F\{^1H\}$ were referenced using the absolute reference function of the MNova 9.0.1 NMR software package. Infrared spectra were recorded on a Nicolet iS10 FT-IR spectrometer. In all dilute 1H NMR spectra, a small, broad artifact is observed at 1.37 ppm; a spectrum of C_6D_6 is provided for reference. When possible, 1H and ^{13}C resonances were assigned using COSY, HSQC, and NOESY experiments. Due to the low solubility and/or thermal stability of some complexes, the signal-to-noise is low in many ^{13}C NMR spectra.

X-ray Crystallography. X-ray crystallographic data were collected on a Rigaku Oxford Diffraction Supernova diffractometer. Crystal samples were handled under immersion oil and quickly transferred to a cold nitrogen stream.

Elemental Analysis. Elemental analyses were performed by Midwest Microlab, LLC.

II. Synthesis and Characterization

$Pd(P(i-BuNCH_2CH_2)_3N)_2$ (1**).** To a 20-mL scintillation vial in the glovebox was added $Pd_2(dba)_3$ (27.4 mg, 0.030 mmol, 1.0 equiv.) and toluene (2 mL). $P(i-BuNCH_2CH_2)_3N$ (46.2 mg, 0.135 mmol, 4.5 equiv.) in toluene (2 mL) was added to the stirred palladium solution. Within 20 min, the solution changed from a dark wine color to a deep burgundy. The reaction mixture was stirred for 16 h, during which time the reaction mixture became green and heterogeneous. The reaction mixture was diluted with toluene until homogeneous, approximately 40 mL, and passed through a pad of Celite to remove solid palladium. The resulting yellow solution was concentrated to a brown solid. The crude solid was suspended in Et_2O , cooled to -35 °C, and the supernatant was then decanted. This suspension-decantation process was repeated until the supernatant was colorless, indicating the absence of dibenzylideneacetone. Residual solvent was evaporated under vacuum to yield the desired complex as an analytically pure, colorless solid (39.6 mg, 0.050 mmol, 83% yield). X-ray quality crystals were grown from a 5:1 Et_2O :toluene mixture at -35 °C. 1H NMR

(500 MHz, C₆D₆): δ 3.33 (ap q, J = 6.1 Hz, 5.64 Hz, 6H, *i*-PrCH₂), 2.87 (br s, 6H, CH₂N_{ax}), 2.75 (t, J = 5.0 Hz, 6H, CH₂N_{eq}), 2.27 (sept, J = 6.8 Hz, 3H, (CH₃)₂CH), 1.14 (d, J = 6.6 Hz, 18H, CH₃); ¹³C NMR (126 MHz, C₆D₆): δ 60.0 (t, J_{C-P} = 16.5 Hz, *i*-PrCH₂), 52.0 (CH₂N_{ax}), 48.0 (CH₂N_{eq}), 29.5 (t, J_{C-P} = 3.00 Hz, Me₂CH), 21.6 (CH₃); ³¹P NMR (202 MHz, C₆D₆): δ 134.5; IR (ATR, cm⁻¹): 2949, 2926, 2823, 1117, 1014, 836, 701; EA Anal. Calcd. for C₃₆H₇₈N₈P₂P: C, 54.63; H, 9.93; N, 14.16. Found: C, 54.30; H, 9.71; N, 14.01.

General Procedure for the Synthesis of Oxidative Addition Complexes (Complexes 2a – 2d). A 20-mL scintillation vial was charged with (COD)Pd(CH₂TMS)₂ (38.9 mg, 0.10 mmol, 1.0 equiv.) and pentane chilled to -35 °C (4 mL). To this solution was added a chilled solution of pentane (8 mL) containing proazaphosphatane (34.2 mg, 0.10 mmol, 1.0 equiv.) and aryl halide (3.0 equiv.). The reaction mixture was stirred for 16 – 18 h at which point the precipitate was permitted to settle and the supernatant was decanted. The resulting solid was again stirred in pentane and the mother liquor decanted. Residual solvent was removed *in vacuo* to yield the desired product. Reactions conducted on a 0.05-mmol scale in (COD)Pd(CH₂TMS)₂ were conducted identically but on half the scale. For all complexes, small quantities of pentane remain despite prolonged exposure to vacuum.

[(N(CH₂CH₂Ni-Bu)₃PPd(C₆H₄-*p*-CN)Br)₂] (2a). This synthesis was performed on a 0.05-mmol scale using the general procedure. The product was isolated as a pale yellow solid (25.2 mg, 0.0399 mmol, 80% yield). X-ray quality crystals were grown from a saturated toluene solution at -35 °C. ¹H NMR (500 MHz, C₆D₆): δ 7.61 (dd, J_{C-P} = 8.0 Hz, 5.3 Hz, 2H, H *meta* to Pd), 6.96 (d, J = 7.8 Hz, 2H, H *para* to Pd), 2.98 (br s, 6H, *i*-PrCH₂), 2.60 (br s, 6H, ethylene CH₂), 2.37 (t, J = 4.8 Hz, 6H, ethylene CH₂), 1.98 (br s, 3H, (CH₃)₂CH), 0.93 (d, J = 6.6 Hz, 18H, CH₃). ¹³C NMR (126 Hz, C₆D₆): δ 161.2 (d, J_{C-P} = 16.1 Hz, CN), 138.4 (d, J = 5.0 Hz, C_{sp2}-H), 129.5 (C_{sp2}-H) 119.9 (*ipso*), 107.4 (*ipso*), 57.7 (br, *i*-PrCH₂), 51.0 (ethylene CH₂), 49.6 (ethylene CH₂), 28.8 (d, J = 3.8 Hz, (CH₃)₂CH), 21.9 (CH₃), Note: one aromatic carbon was not observed; ³¹P NMR (202 MHz, C₆D₆): δ 94.8 ppm; IR (ATR, cm⁻¹): 2954, 2220 (nitrile), 1570, 1470, 1390, 1174, 1031, 811 EA: Anal. Calcd. for C₅₀H₈₆Br₂N₁₀P₂Pd₂: C, 47.59; H, 6.87; N, 11.10 Found: C, 47.43; H, 6.73; N, 11.22.

[(N(CH₂CH₂Ni-Bu)₃PPd(C₆H₄-*p*-CF₃)Br)₂] (2b). This synthesis was performed on a 0.10-mmol scale using the general procedure. The product was isolated as a pale yellow solid (43.6 mg, 0.065 mmol, 65% yield). X-ray quality crystals were grown from a 2:1 pentane:toluene mixture at -20 °C. ¹H NMR (500 MHz, C₆D₆): δ 7.74 (dd, J = 7.9 Hz, 5.4 Hz, 2H, H *meta* to Pd), 7.24 (d, J = 7.9 Hz, 2H, H *ortho* to Pd), 3.04 (br s, 6H, *i*-PrCH₂), 2.62 (br s, 6H, ethylene CH₂), 2.39 (t, J = 5.0 Hz, 6H, ethylene CH₂), 2.00 (br s, 3H, (CH₃)₂CH), 0.98 (d, J = 6.6 Hz, 18 H, CH₃); ¹³C NMR (126 MHz, C₆D₆): δ 137.9 (C *meta* to Pd), 123.4 (C *ortho* to Pd), 57.8 (*i*-PrCH₂), 51.1 (ethylene CH₂), 49.7 (ethylene CH₂), 28.8 ((CH₃)₂CH), 22.0 (CH₃), , Note: *ipso* carbons were not observed; ³¹P NMR (202 MHz, C₆D₆): δ 95.8 ppm; ¹⁹F (282 MHz, C₆D₆): δ -61.6 ppm; IR (ATR, cm⁻¹): 2955, 2927, 2872, 1585, 1390, 1318, 1160, 1037, 1009, 850; Combustion analysis was not pursued since an impurity at 0.58 ppm (¹H NMR) was observed in varying quantities despite recrystallization.

[(N(CH₂CH₂Ni-Bu)₃PPd(C₆H₅-*p*-CN)Br)₂] (2c). This synthesis was performed on a 0.05-mmol scale using the general procedure. The product was isolated as an off-white solid (21.7 mg, 0.0359 mmol, 72% yield). ¹H NMR (500 MHz, C₆D₆): δ 7.71 (t, J = 6.5 Hz, 2H, Ar), 7.03 (t, J =

7.4 Hz, 2H, Ar), 6.87 (t, $J = 7.2$ Hz, 1H, *p*-H), 3.17 (br s, 6H), 2.70 (br s, 6H), 2.46 (t, $J = 5.1$ Hz, 6H), 2.13 (s, 3H, (CH₃)₂CH), 1.04 (d, $J = 6.6$ Hz, 18H, CH₃); ¹³C NMR (126 Hz, C₆D₆): δ 137.8 (d, $J = 5.0$ Hz), 123.1, 58.1, 51.3, 49.6, 28.9, 22.0, Note: Two signals were not observed; ³¹P NMR (202 MHz, C₆D₆): δ 97.6; IR (ATR, cm⁻¹): 2955, 2860, 1561, 1396 1103, 1009, 805. Combustion analysis was not pursued due to the thermal instability of the complex.

[(N(CH₂CH₂Ni-Bu)₃PPd(C₆H₄-*p*-OMe)Br)₂ (2d). This synthesis was performed on a 0.10-mmol scale using the general procedure. The product was isolated as a pale yellow solid (35.6 mg, 0.0560 mmol, 56% yield). ¹H NMR (500 MHz, C₆D₆): δ 7.56 (dd, $J = 8.4, 5.5$ Hz, 2H, Ar), 6.77 (d, $J = 8.2$ Hz, 2H, Ar), 3.38 (s, 3H, OMe), 3.20 (br s, 6H), 2.73 (br s, 6H), 2.47 (ap t, $J = 5.0$ Hz, 6H), 2.15 (br s, 3H, (CH₃)₂CH), 1.05 (d, $J = 6.6$ Hz, 18H, CH₃); ³¹P NMR (202 MHz, C₆D₆): δ 97.5; IR (ATR, cm⁻¹): 2951, 2864, 1480, 1464, 1388, 1183, 1117, 1014, 836; Combustion analysis and ¹³C NMR data were not collected due to the low thermal stability of the complex.

(N(CH₂CH₂Ni-Bu)₃PPd(C₆H₄-*p*-OMe)(N[3,5-CF₃(C₆H₃)]₂) (3). Thawing THF (2 mL) was added to a vial containing complex **2d** (19.8 mg, 0.031 mmol, 1.0 equiv.) and the suspension was frozen in the glovebox cold well. KN[3,5-CF₃(C₆H₃)]₂ (15.5 mg, 0.031 mmol, 1.0 equiv.) was dissolved in THF (4 mL) and layered onto the frozen suspension of **2d**. The suspension was permitted to thaw and mix with the amido salt solution, changing within 30 min from a yellow suspension to a homogeneous, red solution. The reaction mixture was concentrated and the residue was dissolved in pentane. The pentane solution was passed through a syringe filter and the resulting solution was concentrated to saturation. The pentane solution was stored at -35 °C until crystals formed. The supernatant was decanted and residual solvent was removed *in vacuo*, yielding the desired compound as orange crystals (15.5 mg, 0.016 mmol, 50% yield). X-ray quality crystals were grown from a saturated pentane solution at -35 °C. ¹H NMR (500 MHz, C₆D₆): δ 7.91 (s, 4H, *o*-H 3,5-(CF₃)₂C₆H₃), 7.31 (s, 2H, *p*-H 3,5-(CF₃)₂C₆H₃), 7.02 (dd, $J = 8.7, 4.4$ Hz, 2H, anisyl H *ortho* to Pd), 6.45 (d, $J = 8.6$ Hz, 2H, anisyl H *meta* to Pd), 3.21 (s, 3H, OCH₃), 2.66 (dd, $J = 11.4, 7.2$ Hz, 6 H, *i*-PrCH₂), 2.43 – 2.3 (m, 6H, ethylene), 2.32 – 2.24 (m, 6H, ethylene), 1.42 (sept, $J = 6.5$ Hz, 3H, (CH₃)₂CH), 0.80 (d, $J = 6.5$ Hz, 18H, CH₃); ¹³C NMR (126 Hz, C₆D₆): δ 158.6 (*ipso*), 156.1 (*ipso*) 134.6 (anisyl C *ortho* to Pd), 133.0 (*ipso*), 132.8 (*ipso*), 120.7 (*o*-C 3,5-(CF₃)₂C₆H₃), 114.3 (d, $J = 4.0$ Hz, anisyl C *meta* to Pd), 110.9 (*p*-C 3,5-(CF₃)₂C₆H₃) 55.4 (d, $J = 15.4$ Hz, *i*-PrCH₂) 54.9 (OCH₃) 50.4 (ethylene CH₂), 47.8 (ethylene CH₂), 30.2 (*i*-PrCH₂), 20.3 (CH₃), Note: CF₃ not observed; ³¹P NMR (202 MHz, C₆D₆): δ 101.8; ¹⁹F (282 MHz, C₆D₆): δ -62.8; IR (ATR, cm⁻¹): 2951, 1386, 1271, 1161, 1117 EA: Anal. Calcd. for C₄₁H₅₂F₁₂N₅OPPd: C, 49.93; H, 5.26; N, 7.03. Found: C, 49.09; H, 6.01; N, 6.82. Analytically pure material was not obtained despite recrystallization.

III. Reactivity Studies

Use of 2b as a Precatalyst. In a glovebox, **2b** (0.0040 mmol, 2.7 mg, 2 mol %) was dissolved in toluene (1 mL) and added to a vial containing NaOt-Bu (0.300 mmol, 28.8 mg). Additional toluene (1.5 mL) was used to transfer residual **2b**. The reaction mixture immediately became dark pink. To the mixture was added Ph₂NH in toluene (1.5 mL). To the vial a 0.015 M stock solution of **L** (0.015 M in toluene, 0.003 mmol, 200 μ L, 2 mol %) was added followed by 4-bromobenzotrifluoride (0.20 mmol, 28 μ L). The vial was removed from the glovebox and stirred at 80 °C for 16 hours. The reaction mixture became a dark green-black. The mixture was filtered through a medium porosity frit with additional toluene and concentrated on a rotary evaporator to

yield a green-black solid. The crude material was purified by column chromatography (2.5% ethyl acetate/97.5% hexane) to yield a white solid (59.4 mg, 0.190 mmol, 95% yield). ^1H NMR data for the product match that in the literature.⁴

Use of **1 as a Precatalyst.** The above reaction was performed identically but with **1** (3.2 mg, 0.0040 mmol, 2 mol%) in place of **2b**, and without the addition of **L**. The desired product was isolated as a white solid (61.1 mg, 0.195 mmol, 98% yield).

Stoichiometric Coupling of **2b with 4-Bromobenzotrifluoride.** In a glovebox, **2b** (0.010 mmol, 6.7 mg) was dissolved in THF (1 mL) and frozen in a coldwell. The mixture was removed from the coldwell once frozen and to the vial Ph_2NK (0.013 mmol, 2.7 mg) was transferred using THF (2 mL). The reaction mixture was stirred for 15 minutes at ambient temperature. The reaction mixture was stirred for 15 min, during which time it changed from yellow to red to black. The solution was filtered through a syringe filter, the filter was washed with DCM, and the resulting orange solution was concentrated. To the residue was added a stock solution of 1,3,5-trimethoxybenzene in CDCl_3 (200 μL , 0.05 M) and additional CDCl_3 . The yield of $\text{Ph}_2\text{N}(p\text{-C}_6\text{H}_4\text{CF}_3)$ was determined by ^1H NMR relative to the internal standard. First run: 29% yield. Second run: 35% yield.

Acknowledgements

The University of Richmond School of Arts and Sciences, Integrated Quantitative Science program, and Jeffress Memorial Trust are acknowledged for providing summer fellowships in support of this work. Other contributors include Gregory Gravalis, who carried out preliminary studies, and Dr. Nathan Schley (Vanderbilt University) who conducted the X-ray crystallography analysis. None of this work would have been possible without Dr. Miles Johnson, whose patience, mentorship, and sense of humor carried me through much of my time as a student at UR.

References

- (1) Busacca, C. A.; Fandrick, D. R.; Song, J. J.; Senanayake, C. H. The Growing Impact of Catalysis in the Pharmaceutical Industry. *Advanced Synthesis & Catalysis* **2011**, 353 (11–12), 1825–1864.
- (2) Torborg, C.; Beller, M. Recent Applications of Palladium-Catalyzed Coupling Reactions in the Pharmaceutical, Agrochemical, and Fine Chemical Industries. *Advanced Synthesis & Catalysis* **2009**, 351, 3027–3043.
- (3) Roughley, S. D.; Jordan, A. M. The Medicinal Chemist's Toolbox: An Analysis of Reactions Used in the Pursuit of Drug Candidates. *Journal of Medicinal Chemistry* **2011**, 54 (10), 3451–3479.
- (4) Johansson Seechurn, C. C. C.; Kitching, M. O.; Colacot, T. J.; Snieckus, V. Palladium-Catalyzed Cross-Coupling: A Historical Contextual Perspective to the 2010 Nobel Prize. *Angewandte Chemie* **2012**, 51, 5062–5085.
- (5) Altenhoff, G.; Goddard, R.; Lehmann, C. W.; Glorius, F. An N-Heterocyclic Carbene Ligand with Flexible Steric Bulk Allows Suzuki Cross-Coupling of Sterically Hindered Aryl Chlorides at Room Temperature. *Angewandte Chemie International Edition* **2003**, 42 (31), 3690–3693.
- (6) Verkade, J. G. Atranes: New Examples with Unexpected Properties. *Accounts of Chemical Research* **1993**, 26, 483–489.

- (7) Thammavongsy, Z.; Kha, I. M.; Ziller, J. W.; Yang, J. Y. Electronic and Steric Tolman Parameters for Proazaphosphatranes, the Superbase Core of the Tri(Pyridylmethyl)Azaphosphatrane (TPAP) Ligand. *Dalton Trans* **2016**, *45*, 9853–9859.
- (8) Urgaonkar, S.; Nagarajan, M.; Verkade, J. G. P(i-BuNCH₂CH₂)₃N: An Effective Ligand in the Palladium-Catalyzed Amination of Aryl Bromides and Iodides. *Journal of Organic Chemistry* **2003**, *68*, 452–459.
- (9) Urgaonkar, S.; Verkade, J. G. Scope and Limitations of Pd₂(Dba)₃/P(i-BuNCH₂CH₂)₃N-Catalyzed Buchwald-Hartwig Amination Reactions of Aryl Chlorides. *Journal of Organic Chemistry* **2004**, *69*, 9135–9142.
- (10) Urgaonkar, S. M.; Nagarajan, M.; Verkade, J. G. Pd/P(i-BuNCH₂CH₂)₃N: An Efficient Catalyst for Suzuki Cross-Coupling of Aryl Bromides and Chlorides with Arylboronic Acids. *Tetrahedron Letters* **2002**, *43* (49), 8921–8924.
- (11) Su, W.; Urgaonkar, S.; McLaughlin, P. A.; Verkade, J. G. Highly Active Palladium Catalysts Supported by Bulky Proazaphosphatrane Ligands for Stille Cross-Coupling: Coupling of Aryl and Vinyl Chlorides, Room Temperature Coupling of Aryl Bromides, Coupling of Aryl Triflates, and Synthesis of Sterically Hindered Biaryls. *Journal of the American Chemical Society* **2004**, *126* (50), 16433–16439.
- (12) Matthews, A. D.; Gravalis, G. M.; Schley, N. D.; Johnson, M. W. Synthesis, Structure, and Reactivity of Palladium Proazaphosphatrane Complexes Invoked in C–N Cross Coupling. *Organometallics* **2018**, *37*, 3073–3078.
- (13) Shekhar, S.; Ryberg, P.; Hartwig, J. F.; Mathew, J. S.; Blackmond, D. G.; Strieter, E. R.; Buchwald, S. L. Reevaluation of the Mechanism of the Amination of Aryl Halides Catalyzed by BINAP-Ligated Palladium Complexes. *Journal of the American Chemical Society* **2006**, *128*, 3584–3591.
- (14) Hooper, M. H.; Utsunomiya, M.; Hartwig, J. F. Scope and Mechanism of Palladium-Catalyzed Amination of Five-Membered Heterocyclic Halides. *Journal of Organic Chemistry* **2003**, *68* (7), 2861–2873.
- (15) Paul, F.; Patt, J.; Hartwig, J. F. Structural Characterization and Simple Synthesis of {Pd[P(o-Tol)₃]₂}, Dimeric Palladium(II) Complexes Obtained by Oxidative Addition of Aryl Bromides, and Corresponding Monometallic Amine Complexes. *Organometallics* **1995**, *14*, 3030–3039.
- (16) Widenhoefer, R. A.; Buchwald, S. L. Halide and Amine Influence in the Equilibrium Formation of Palladium Tris(o-Tolyl)Phosphine Mono(Amine) Complexes from Palladium Aryl Halide Dimers. *Organometallics* **1996**, *15*, 2755–2763.
- (17) Arrechea, P. L.; Buchwald, S. L. Biaryl Phosphine Based Pd(II) Amido Complexes: The Effect of Ligand Structure on Reductive Elimination. *Journal of the American Chemical Society* **2016**, *138*, 12486–12493.
- (18) Matthews, A. D.; Prasad, S.; Schley, N. D.; Donald, K. J.; Johnson, M. W. On Transannulation in Azaphosphatranes: Synthesis and Theoretical Analysis. *Inorganic Chemistry* **2019**, *58* (23), 15983–15992.
- (19) Glock, C.; Görls, H.; Westerhausen, M. Electronic, Steric, and Ligand Influence on the Solid-State Structures of Substituted Sodium and Potassium Anilides. *European Journal of Inorganic Chemistry* **2011**, *34*, 5288–5298.
- (20) Yamashita, M.; Hartwig, J. F. Synthesis, Structure, and Reductive Elimination Chemistry of Three-Coordinate Arylpalladium Amido Complexes. *Journal of the American Chemical Society* **2004**, *126*, 5344–5345.

- (21) Cheng, G.; Luo, M. Homocoupling of Arylboronic Acids Catalyzed by CuCl in Air at Room Temperature. *European Journal of Inorganic Chemistry* **2011**, 2011 (13), 2519–2523.

Supporting Information

I. Byproduct Profiles and Half-Life Determination

Byproduct profile



The presence of byproducts is reported based on observations from the half-life determination experiments.

	2a	2b	2c	2d	3
1	Not Detected	Not Detected	Detected	Detected	Detected
Biaryl	Detected	Detected	Detected	Detected	Not Detected
ArX	Not Detected	Not Detected	Not Detected	Not Detected	Not Detected
L	Not Detected	Not Detected	Not Detected	Not Detected	Not Detected

Half-life Determination

A J. Young tube was charged with complexes **2a** - **2d** (0.005 mmol), 1,3,5-trimethoxybenzene (0.5 mg, 0.003 mmol), and C₆D₆ (0.6 mL). ¹H NMR spectra were taken to establish the duration of the first half-life for each complex relative to the internal standard. Each half-life measurement was performed in duplicate. In the case of **2b**, 0.003 mmol of the complex was used due to low solubility.

II. NMR Spectra

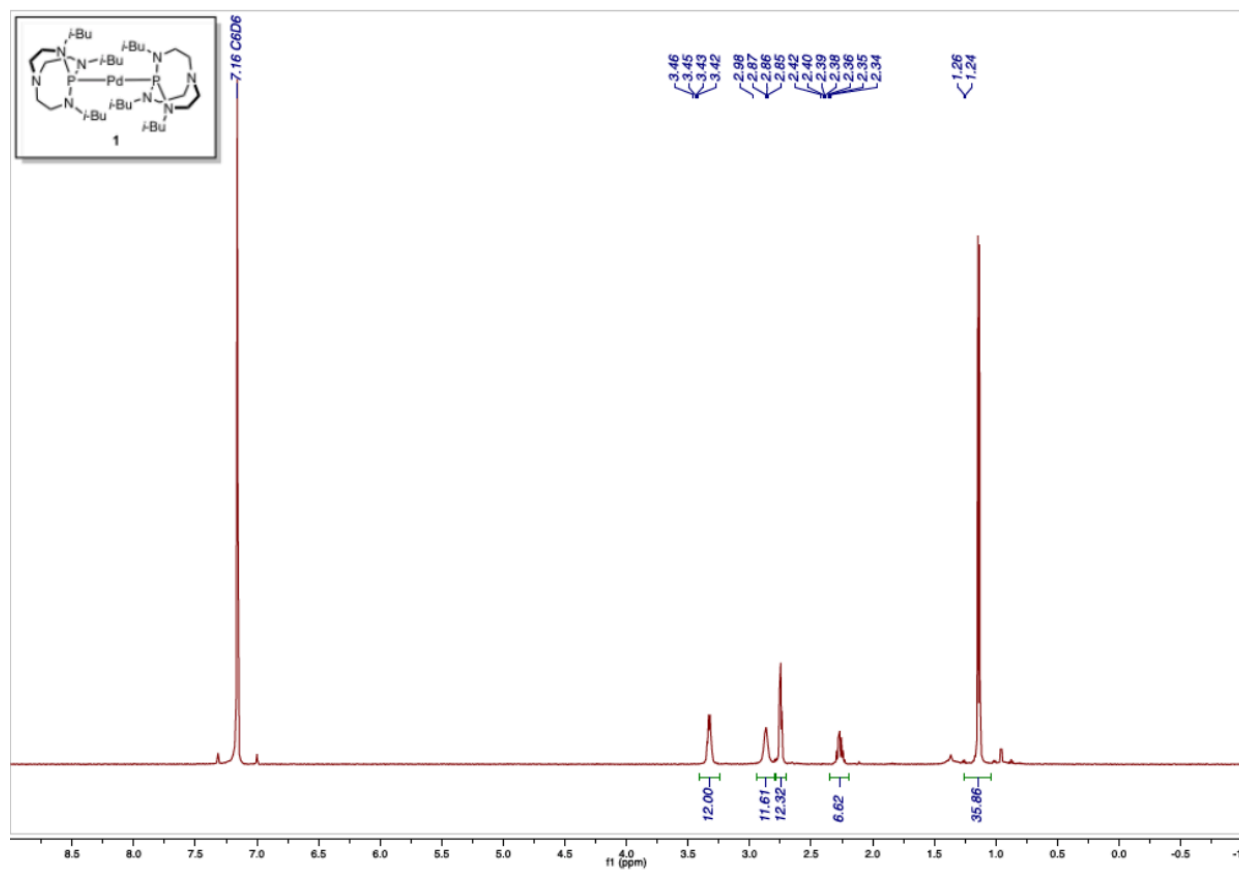


Figure S1. ^1H NMR spectrum of Complex 1.

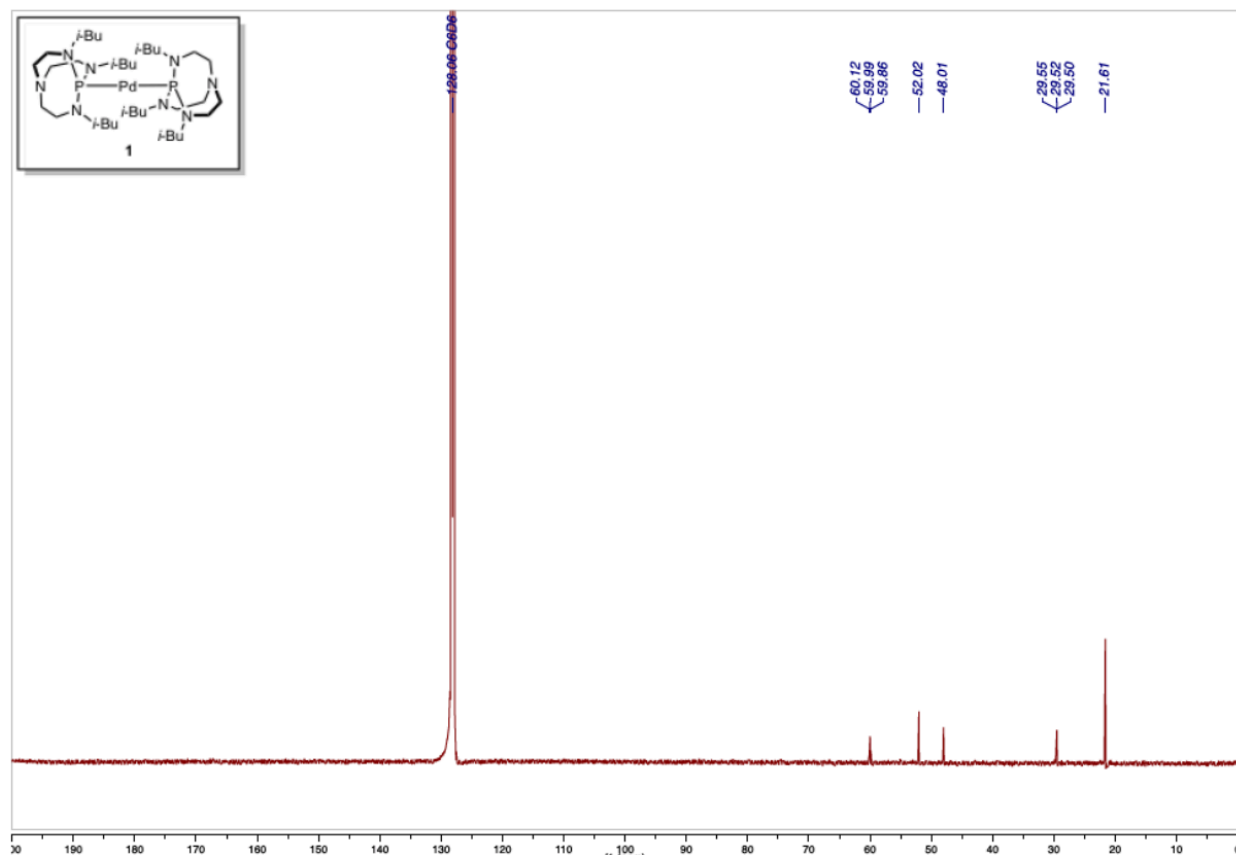


Figure S2. $^{13}\text{C}\{\text{H}\}$ NMR spectrum of Complex **1**.

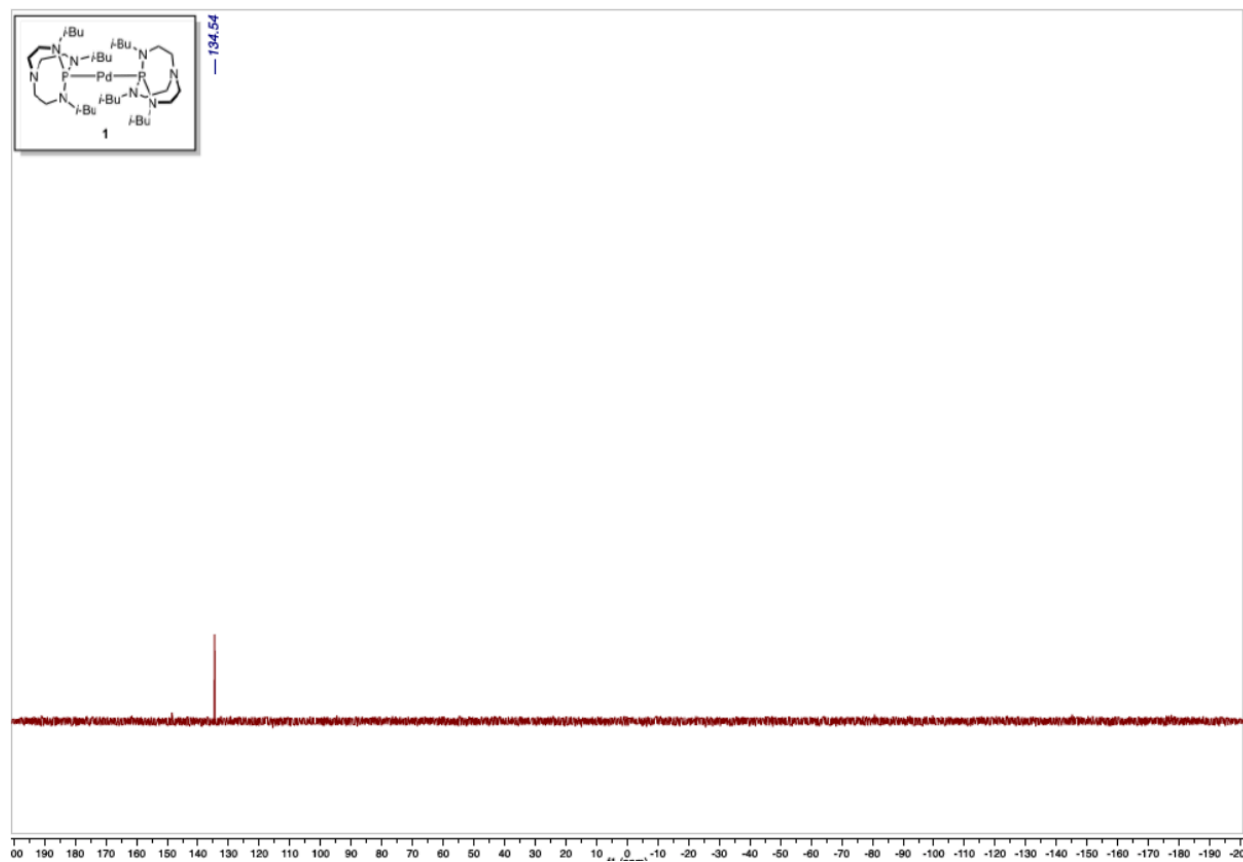


Figure S3. $^{31}\text{P}\{\text{H}\}$ NMR spectrum of Complex 1.

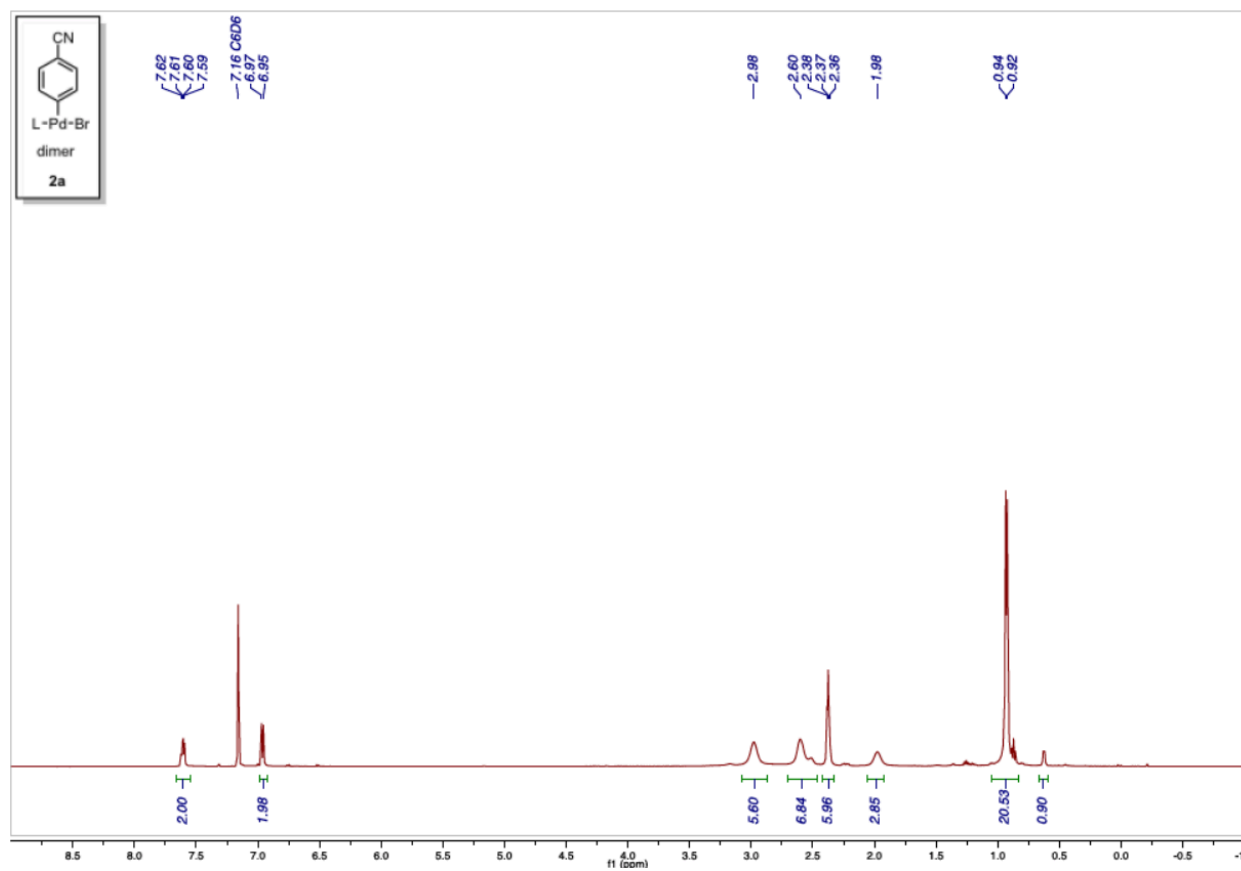


Figure S4. ¹H NMR spectrum of Complex **2a**.

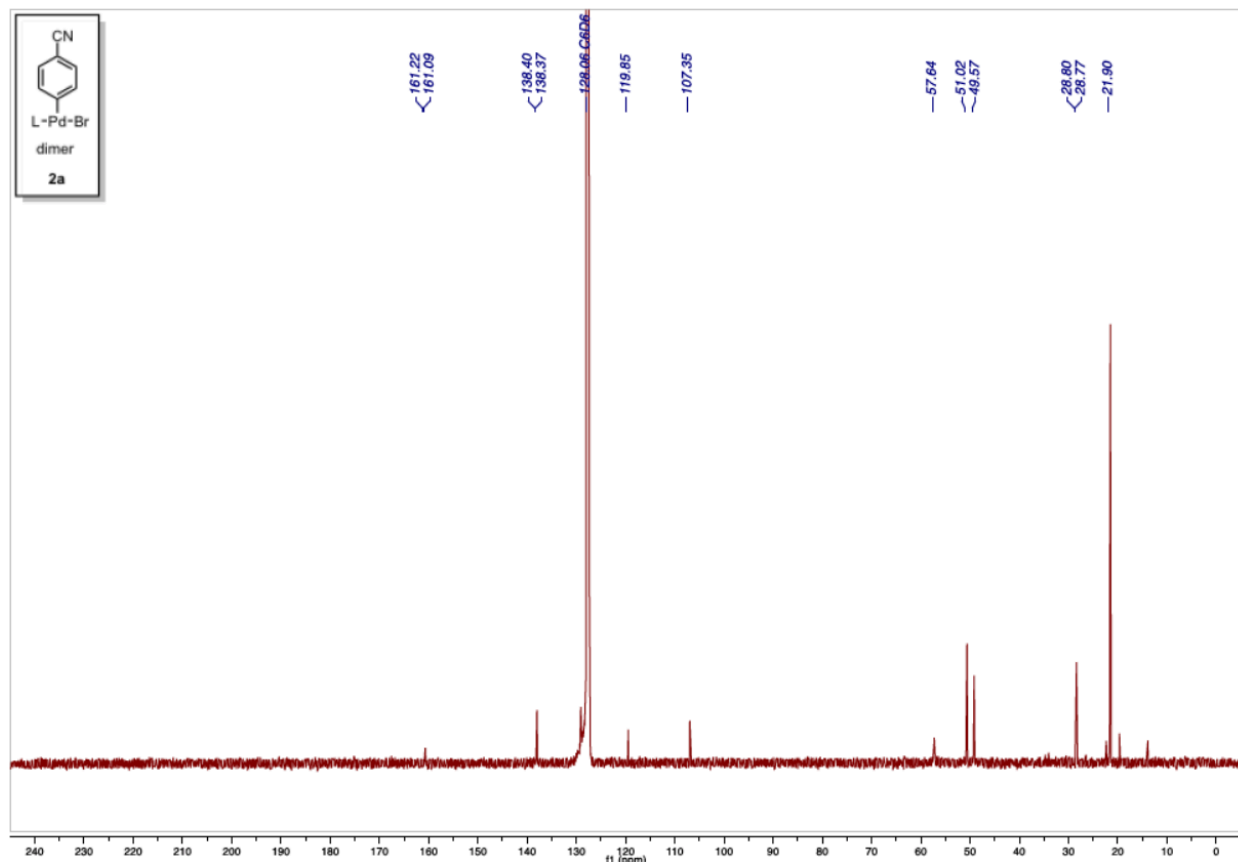


Figure S5. $^{13}C\{H\}$ NMR spectrum of Complex 2a.

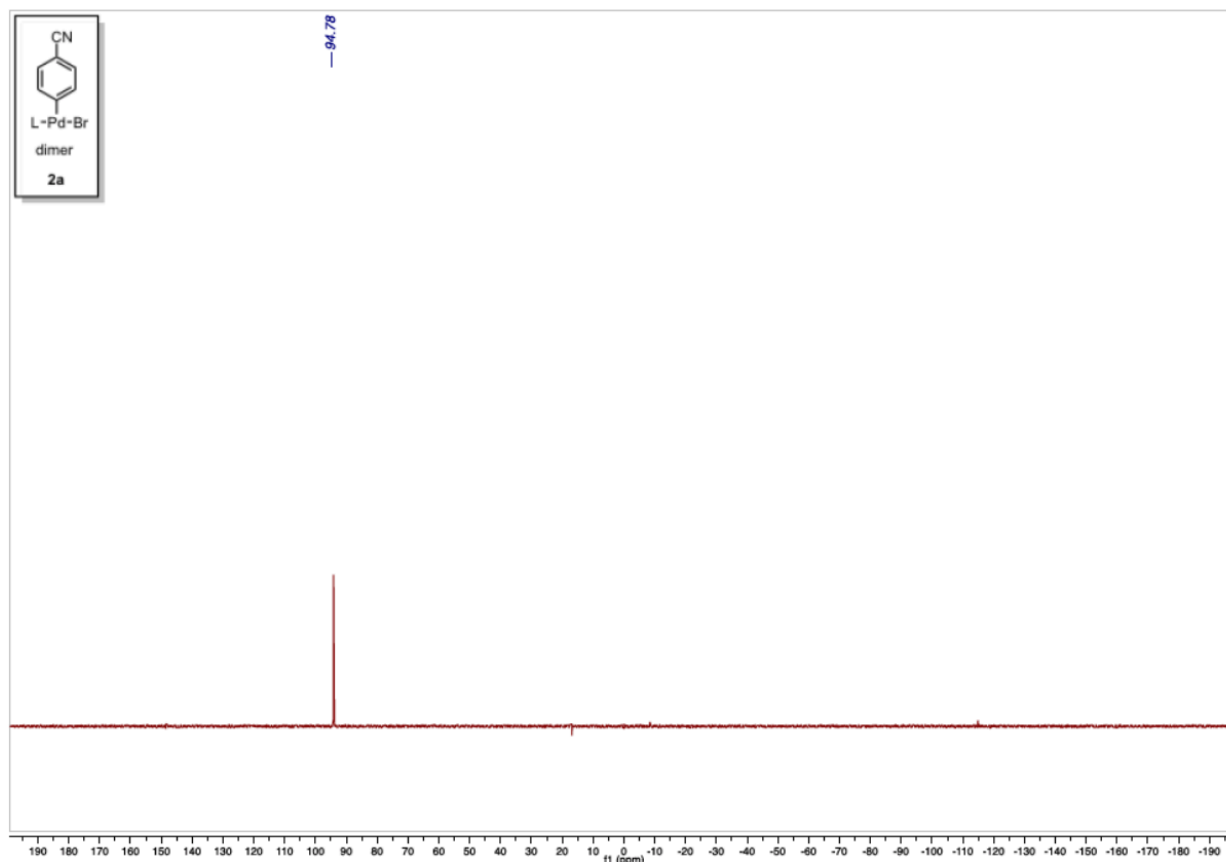


Figure S6. $^{31}\text{P}\{\text{H}\}$ NMR spectrum of Complex 2a.

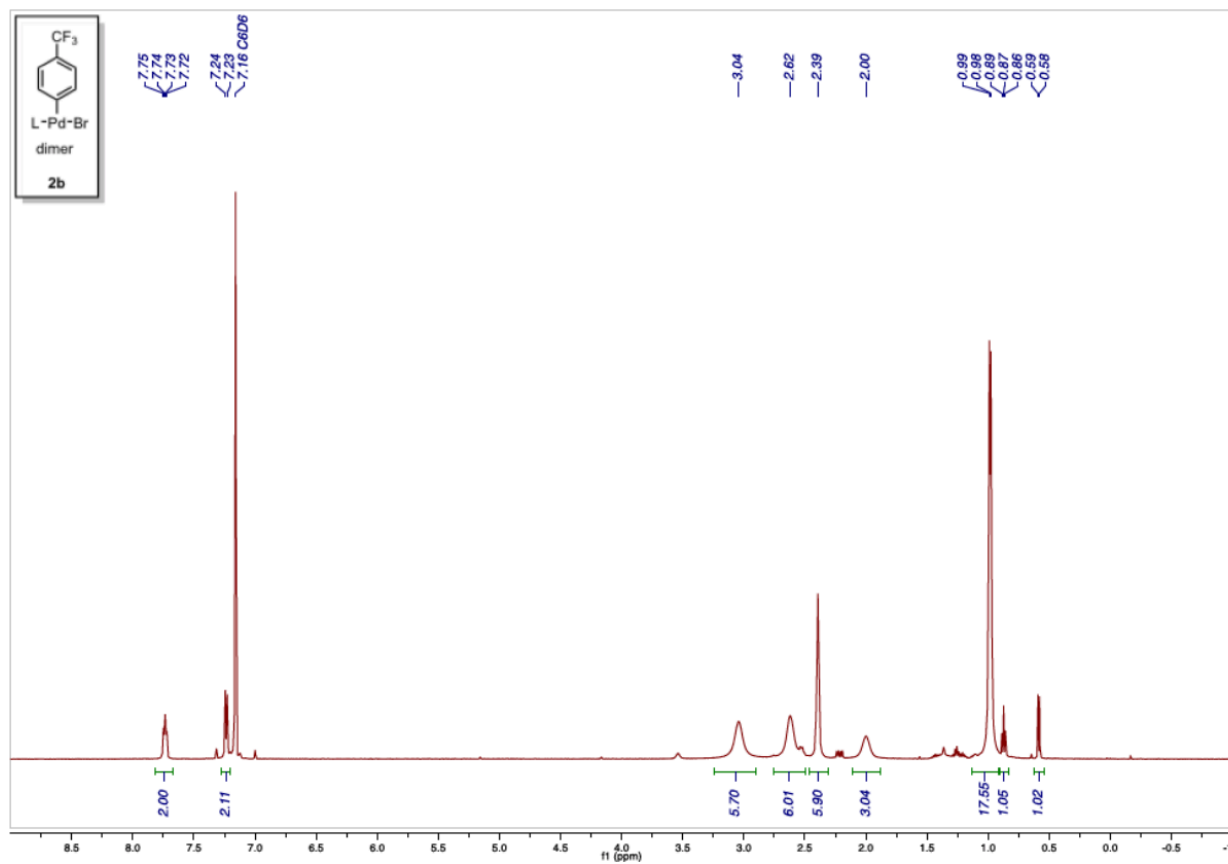


Figure S7. ¹H NMR spectrum of Complex **2b**.

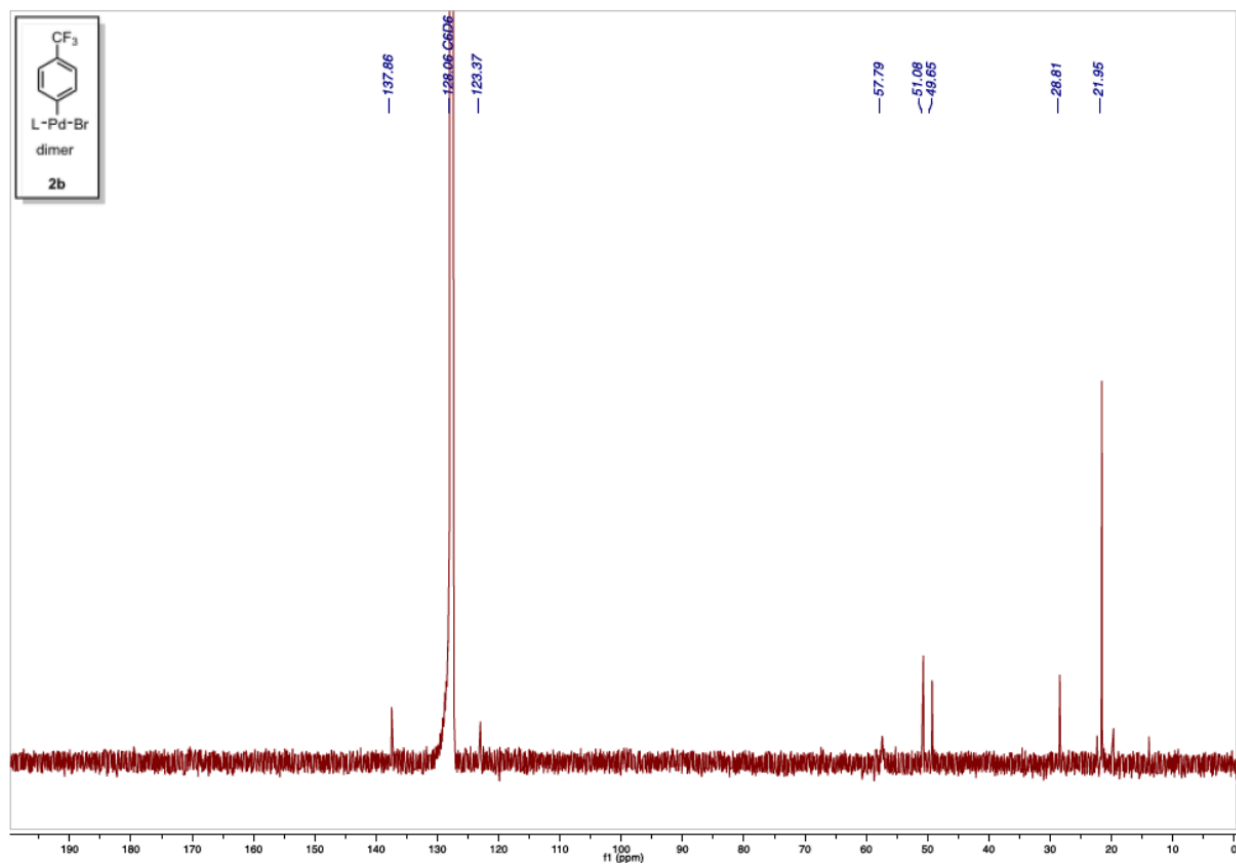


Figure S8. $^{13}\text{C}\{\text{H}\}$ NMR spectrum of Complex **2b**.

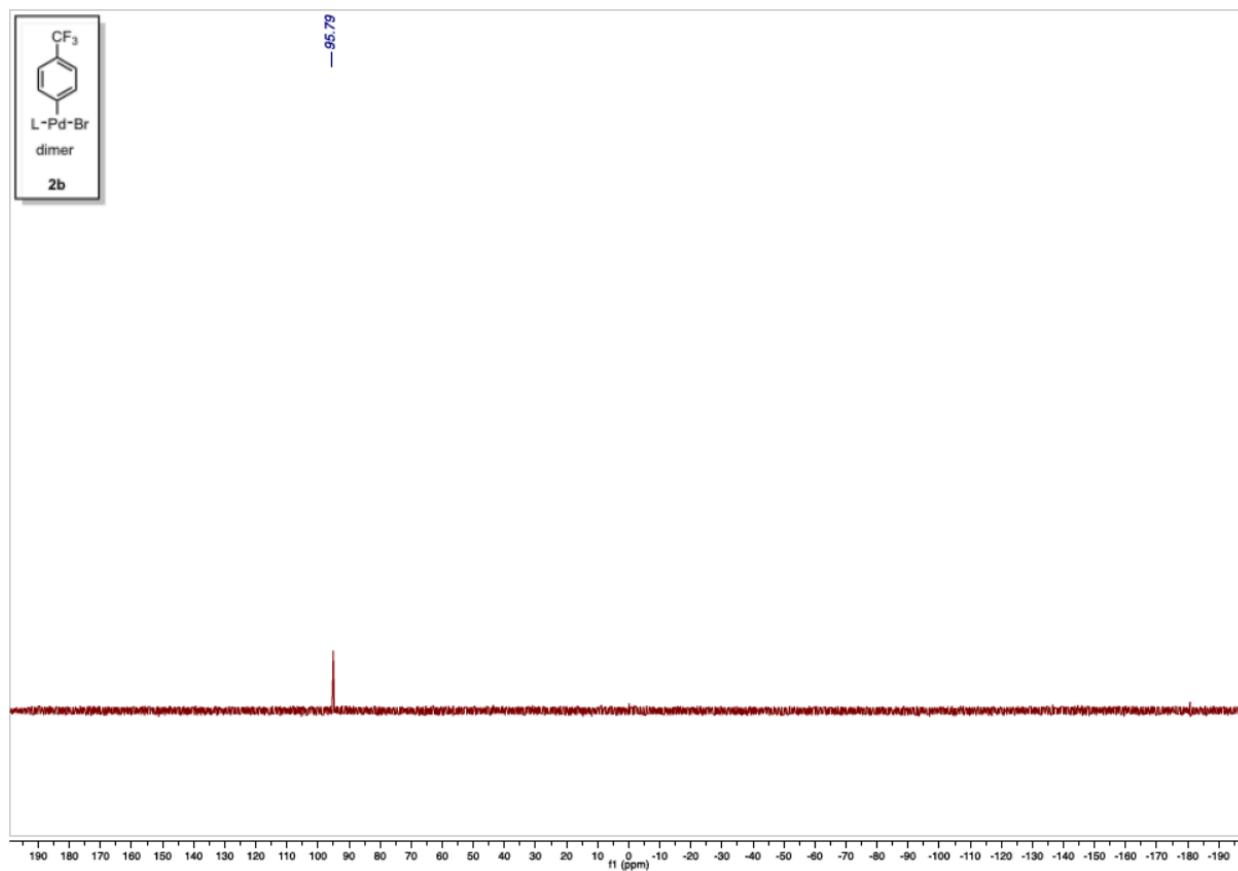


Figure S9. $^{31}\text{P}\{\text{H}\}$ NMR spectrum of Complex **2b**.

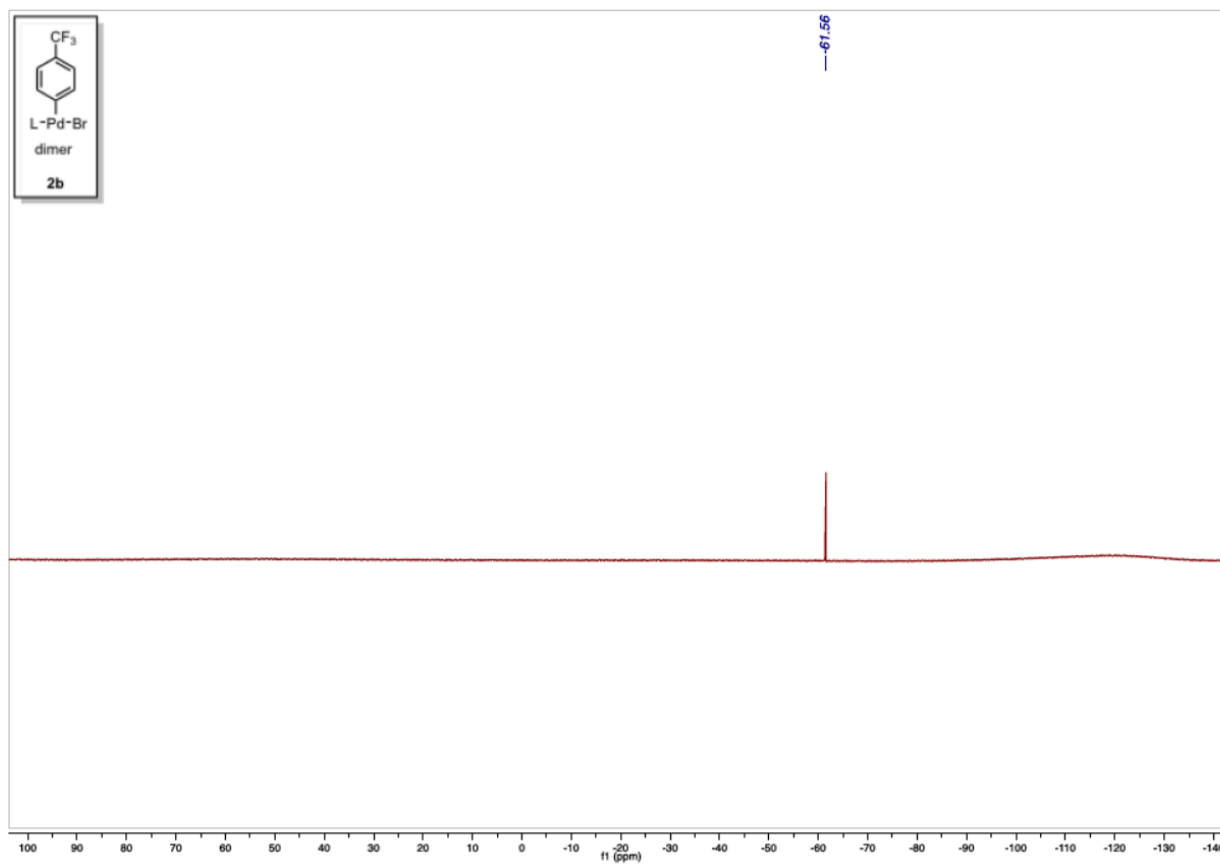


Figure S10. $^{19}\text{F}\{^1\text{H}\}$ NMR spectrum of Complex **2b**.

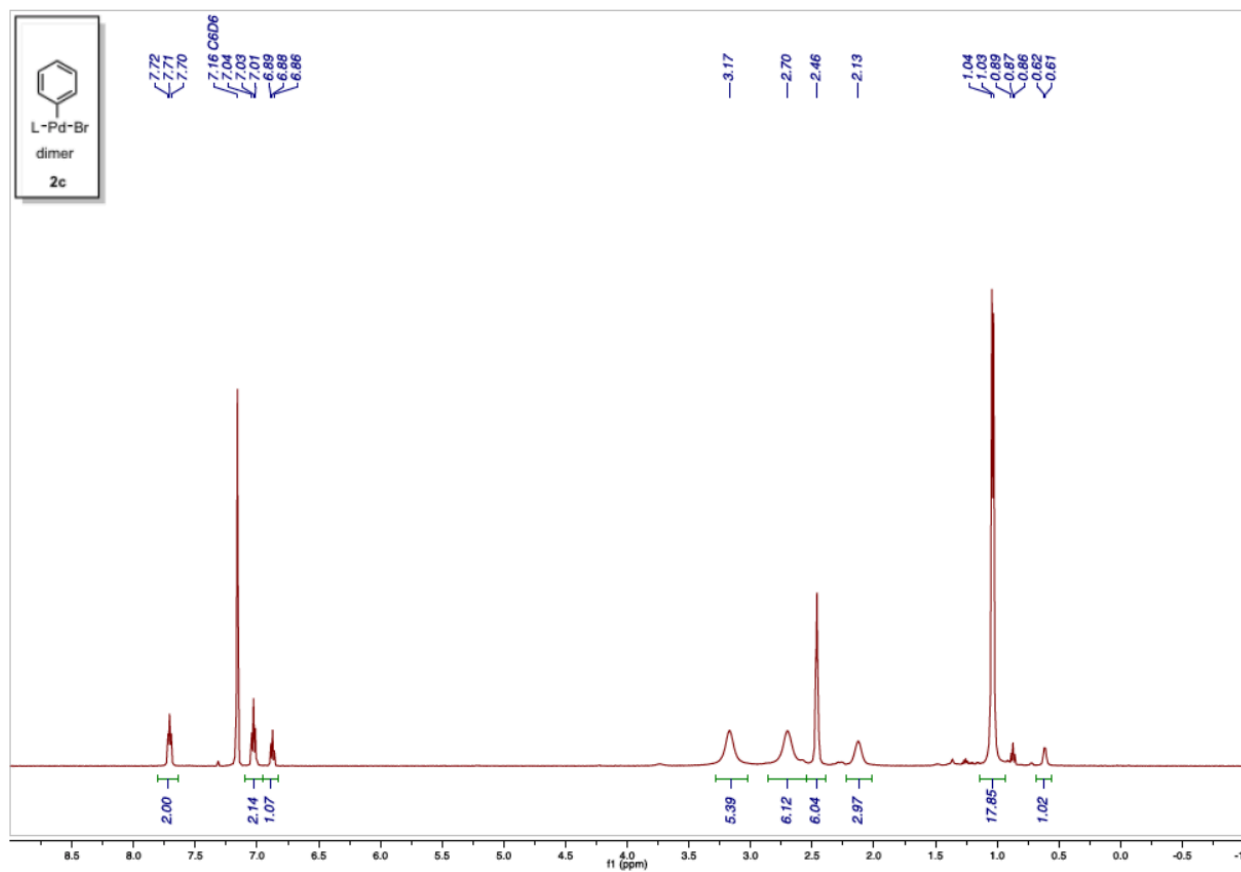


Figure S11. ^1H NMR spectrum of Complex **2c**.

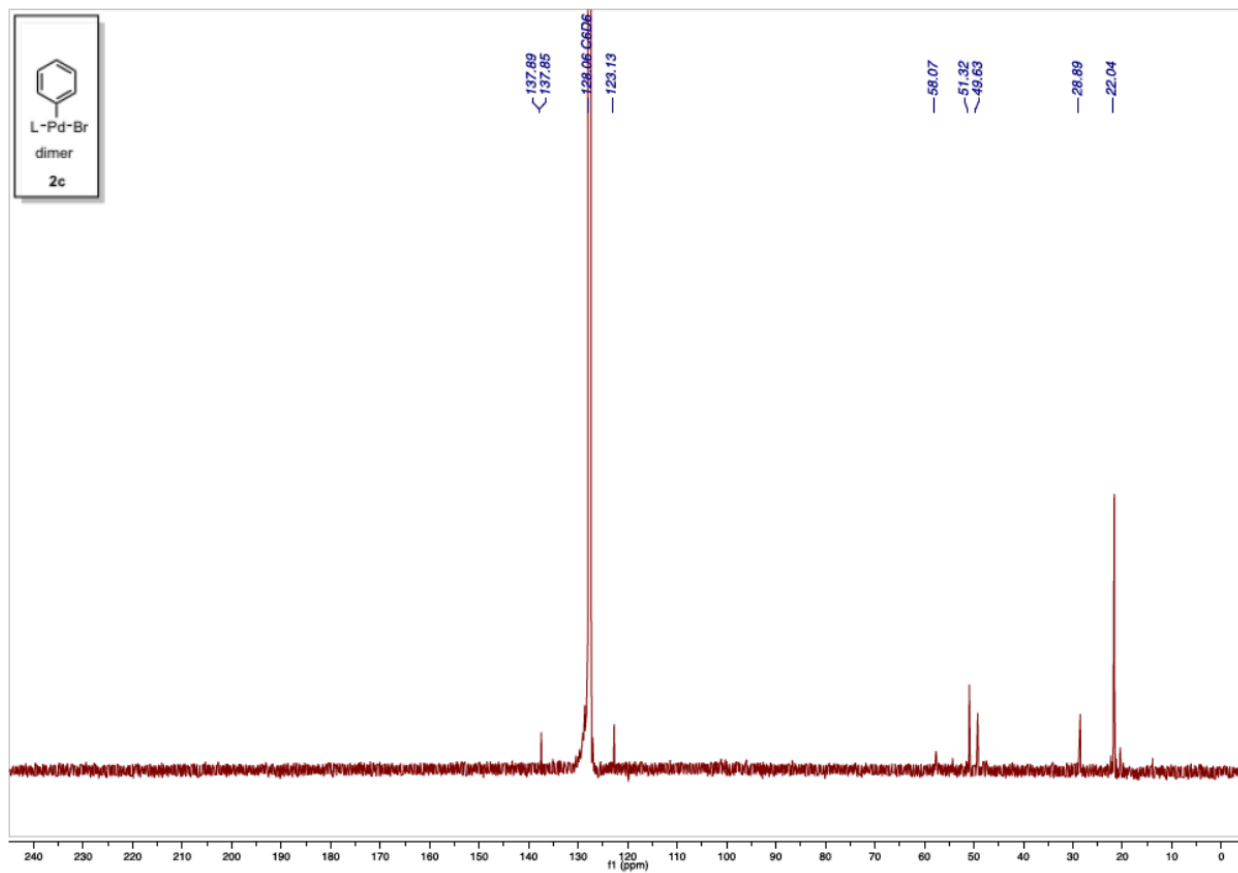


Figure S12. $^{13}\text{C}\{\text{H}\}$ NMR spectrum of Complex **2c**.

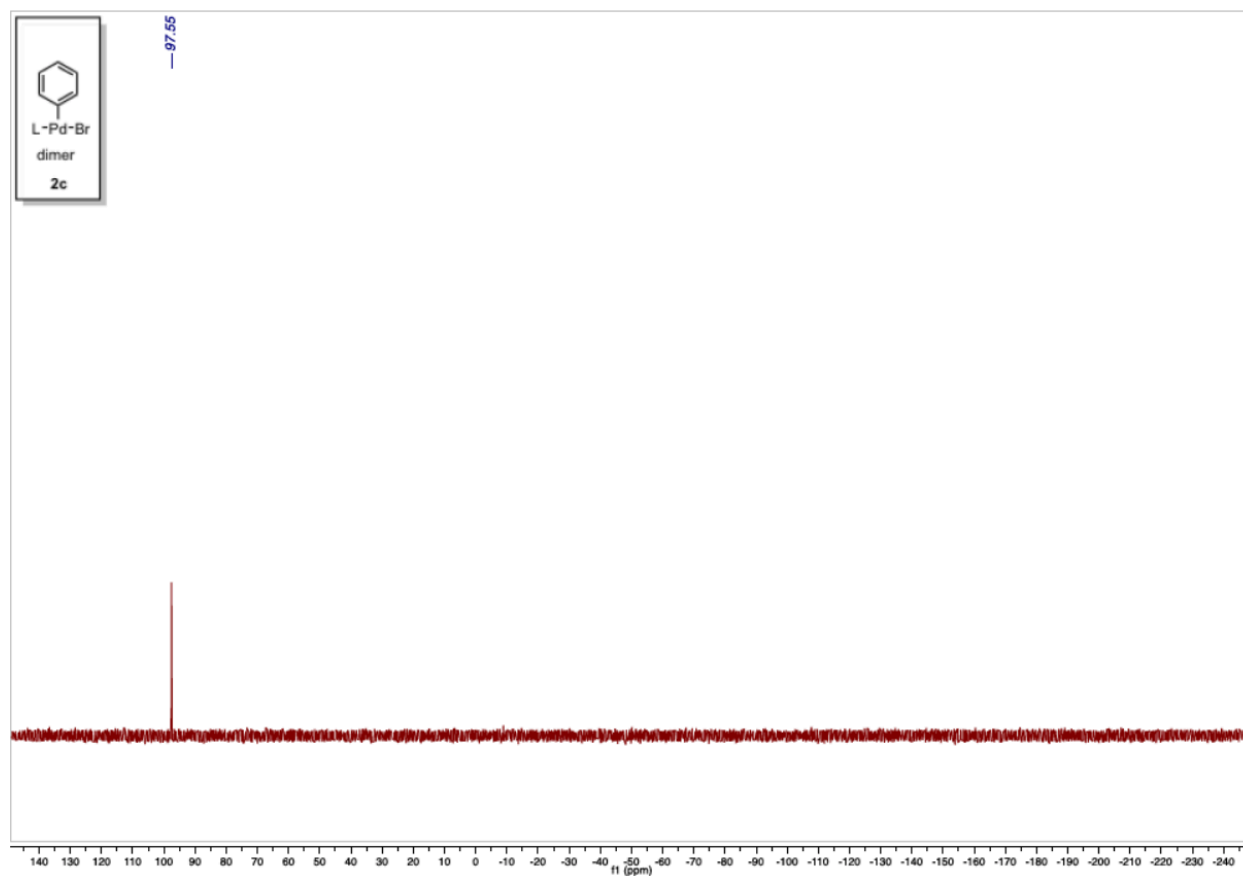


Figure S13. $^{31}\text{P}\{\text{H}\}$ NMR spectrum of Complex **2c**.

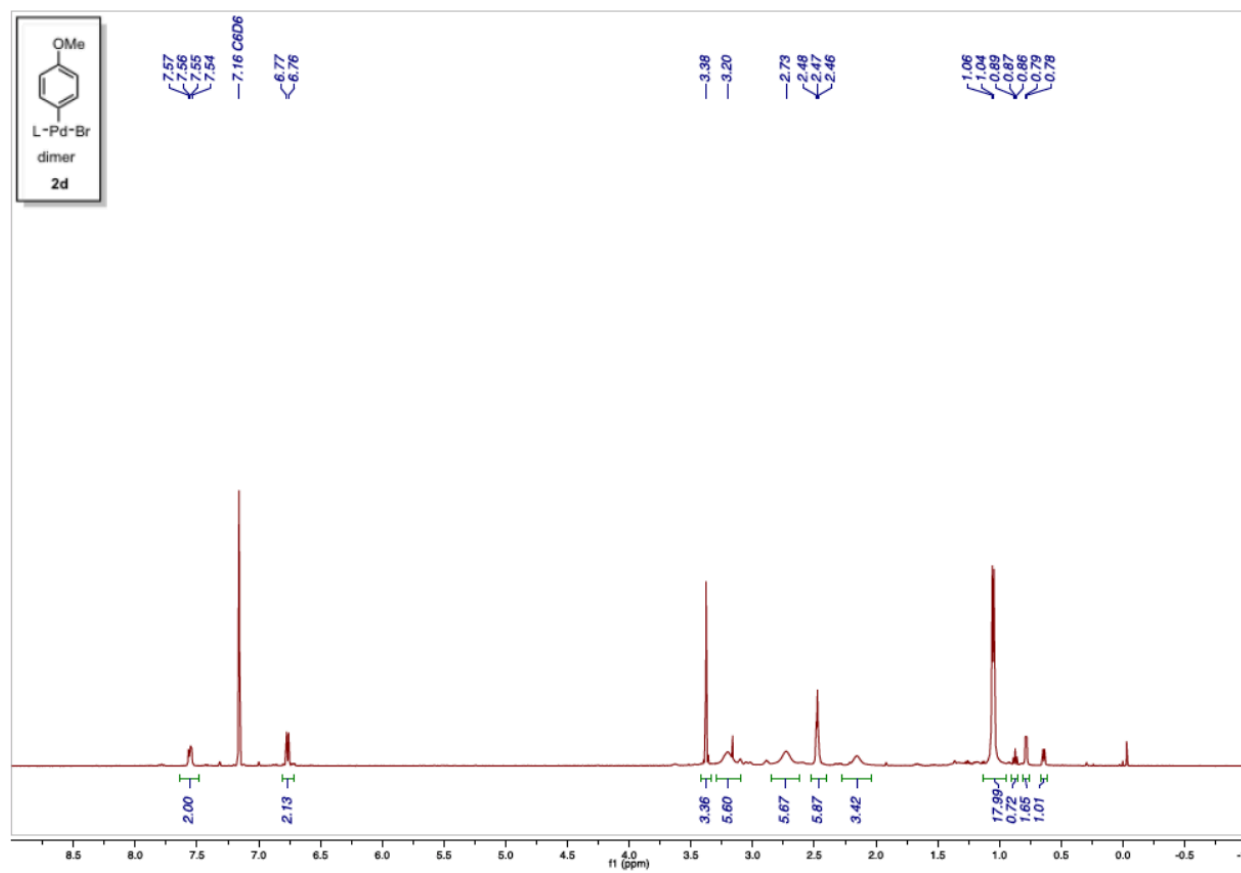


Figure S14. 1H NMR spectrum of Complex **2d**.

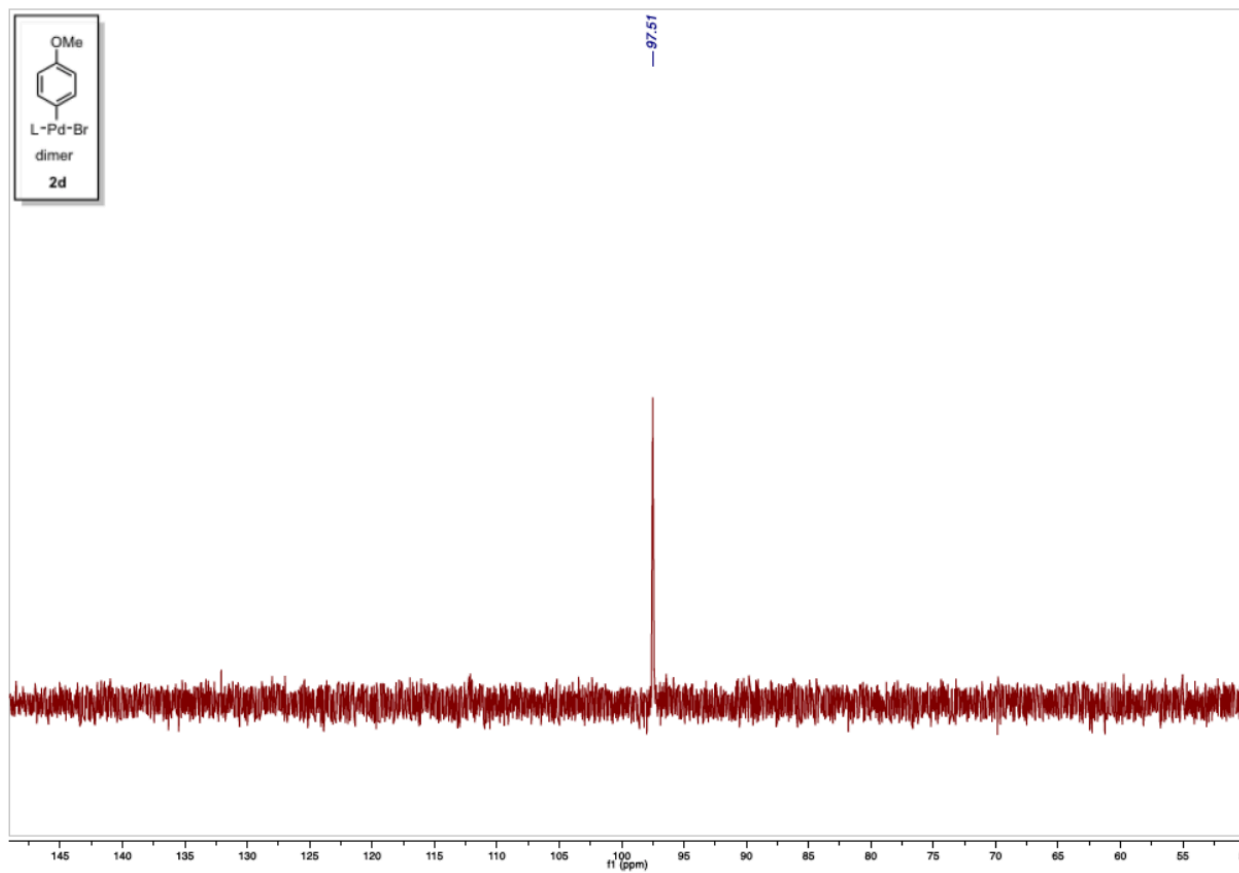


Figure S15. $^{13}\text{P}\{\text{H}\}$ NMR spectrum of Complex **2d**.

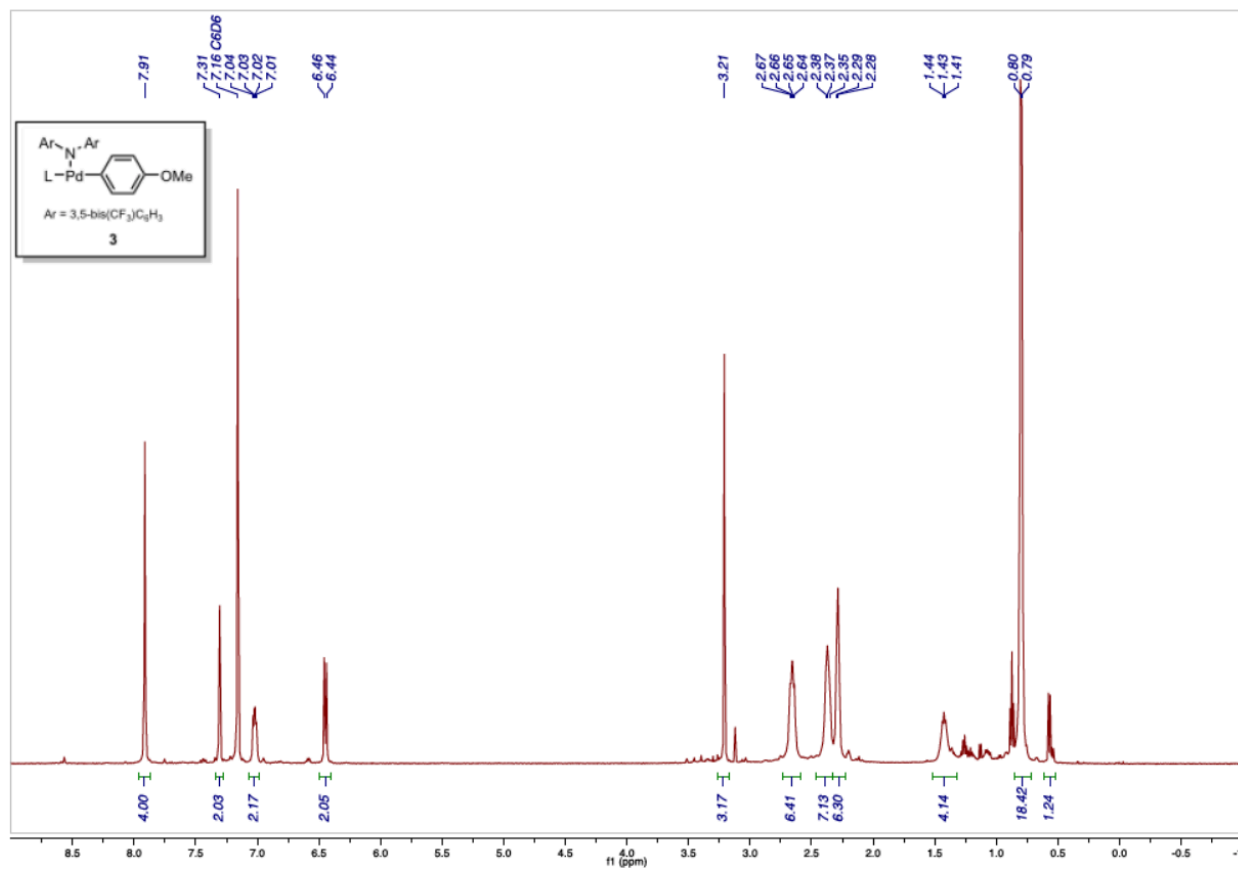


Figure S16. ¹H NMR spectrum of Complex **3**.

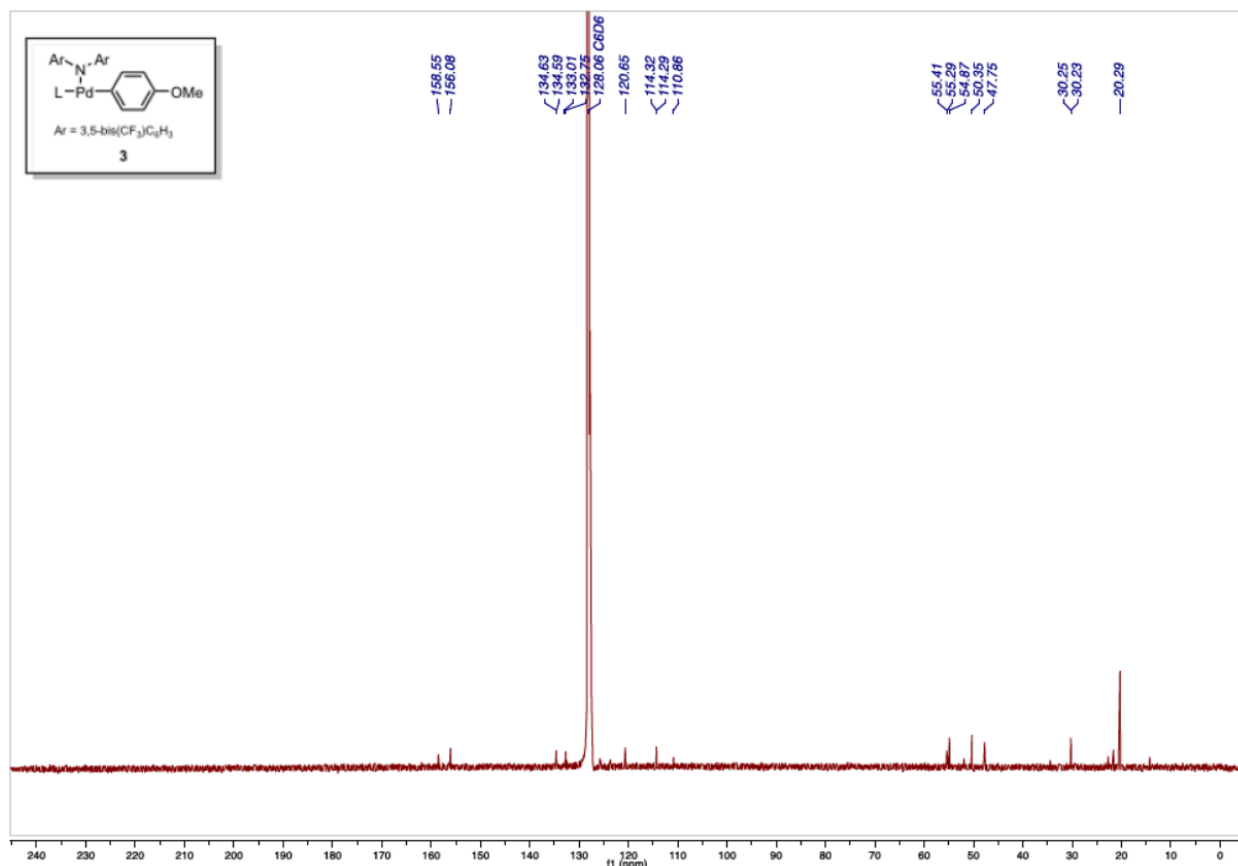


Figure S17. ¹³C{H} NMR spectrum of Complex 3.

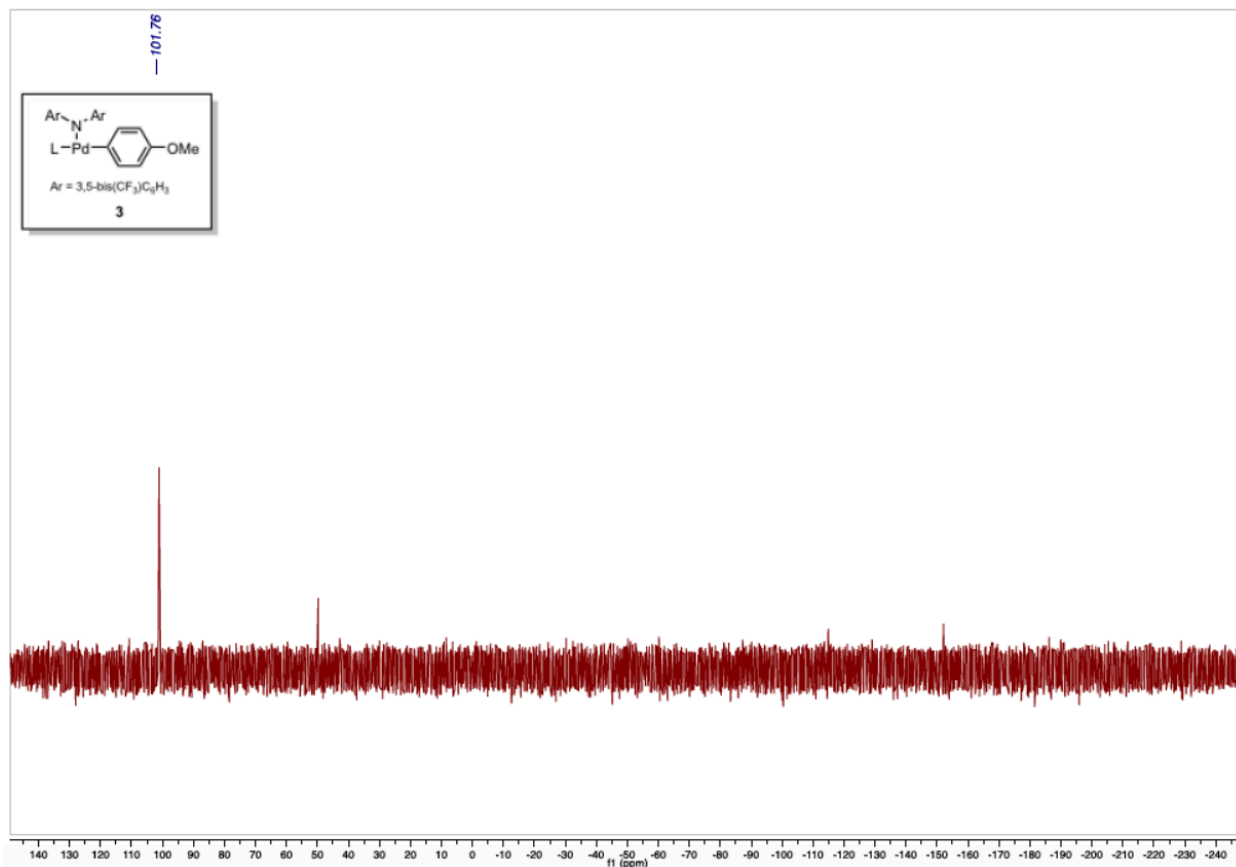


Figure S18. $^{31}\text{P}\{\text{H}\}$ NMR spectrum of Complex **3**.

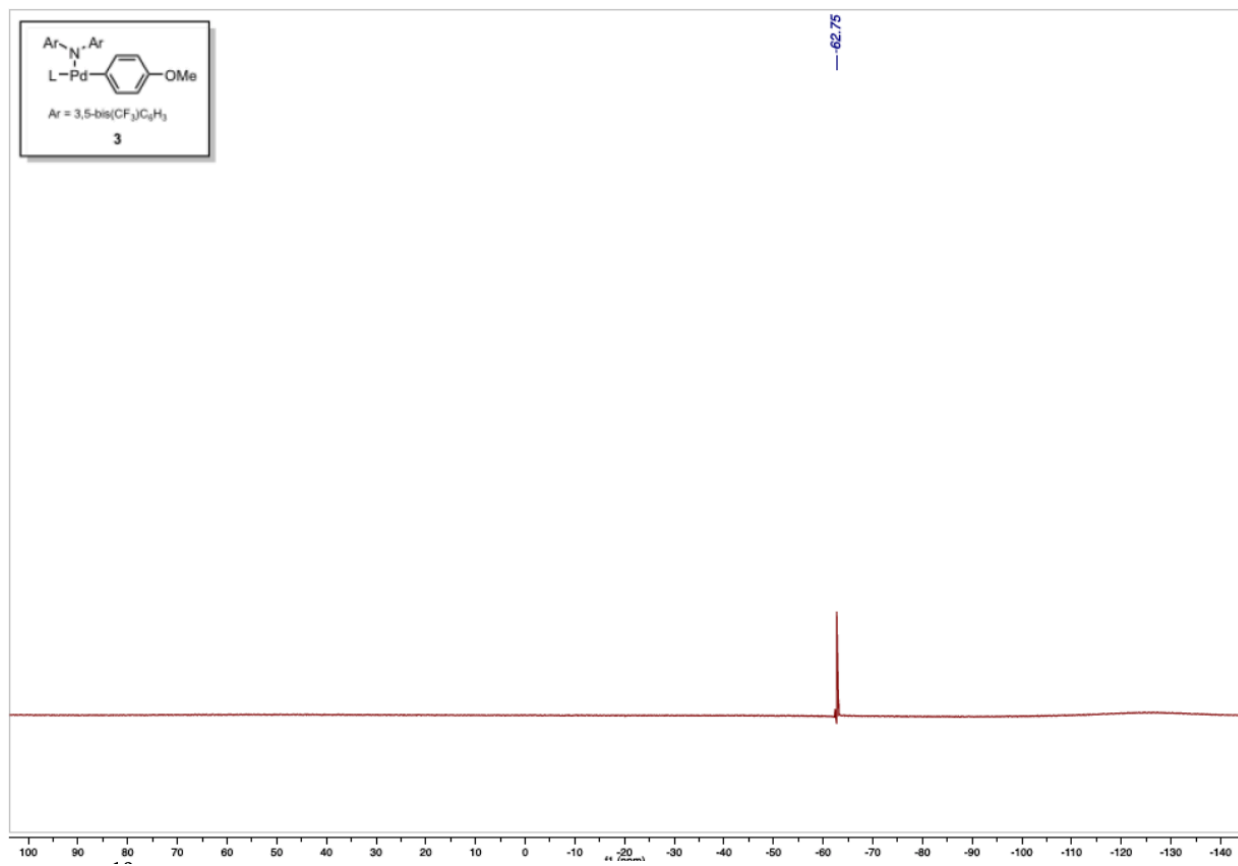


Figure S19. $^{19}\text{F}\{\text{H}\}$ NMR spectrum of Complex **3**.

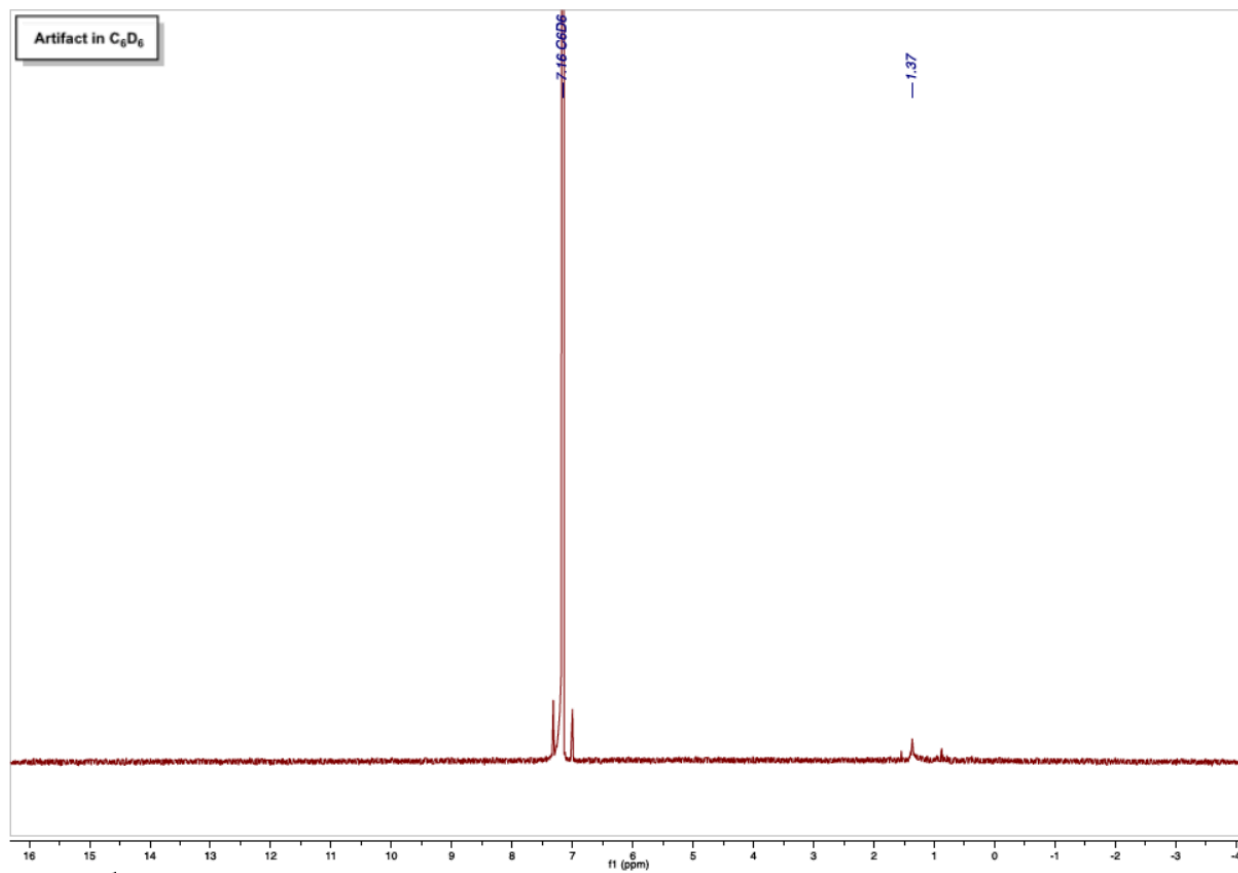


Figure S20. ^1H NMR spectrum of artifact present in C_6D_6 .

III. X-Ray Crystallographic Data

Table 1. Crystal data and structure refinement for **1**.

Identification code	1850176
Empirical formula	C ₃₆ H ₇₈ N ₈ P ₂ Pd
Formula Weight	791.38
Temperature	100.0(2) K
Wavelength	0.71073 Å
Crystal system	Trigonal
Space group	R $\bar{3}$ c
Unit cell dimensions	a = 12.2939(2) Å $\alpha = 90^\circ$ b = 12.2939(2) Å $\beta = 90^\circ$ c = 45.6661(11) Å $\gamma = 120^\circ$
Volume	5977.3(3) Å ³
Z	6
Density (calculated)	1.319 Mg/m ³
Absorption coefficient	0.582 mm ⁻¹
F(000)	2556
Crystal size	0.199 x 0.107 x 0.048 mm ³
Theta range for data collection	3.314 to 29.348°
Index ranges	-16 ≤ h ≤ 16, -16 ≤ k ≤ 16, -61 ≤ l ≤ 55
Reflections collected	13481
Independent reflections	1721 [R(int) = 0.0284]
Completeness to theta = 25.242°	99.8%
Absorption correction	Gaussian
Max. and min. transmission	1.000 and 0.726
Refinement method	Full-matrix least squares on F ²
Data / restraints / parameters	1721 / 0 / 74
Goodness-of-fit on F ²	1.087
Final R indices [I > 2σ(I)]	R1 = 0.0238, wR2 = 0.0552
R indices (all data)	R1 = 0.0273, wR2 = 0.0569
Largest diff. peak and hole	0.390 and -0.453 e/Å ⁻³

Table 2. Crystal data and structure refinement for **2a**.

Identification code	1850178
Empirical formula	C ₆₄ H ₁₀₂ Br ₂ N ₁₀ P ₂ Pd
Formula Weight	1446.11
Temperature	100.01(10) K
Wavelength	1.54184 Å
Crystal system	Monoclinic
Space group	P 1 21/ n 1
Unit cell dimensions	a = 27.8217(3) Å $\alpha = 90^\circ$ b = 10.98822(12) Å $\beta = 105.5009(13)^\circ$ c = 45.5149(6) Å $\gamma = 90^\circ$
Volume	13408.3(3) Å ³
Z	8
Density (calculated)	1.433 Mg/m ³
Absorption coefficient	6.522 mm ⁻¹
F(000)	5984
Crystal size	0.186 x 0.129 x 0.117 mm ³
Theta range for data collection	3.032 to 72.363°
Index ranges	-34 ≤ h ≤ 34, -13 ≤ k ≤ 13, -54 ≤ l ≤ 56
Reflections collected	99636
Independent reflections	26178 [R(int) = 0.0474]
Completeness to theta = 25.242°	100.0%
Absorption correction	Gaussian
Max. and min. transmission	1.000 and 0.798
Refinement method	Full-matrix least squares on F ²
Data / restraints / parameters	26178 / 594 / 1594
Goodness-of-fit on F ²	1.125
Final R indices [I > 2sigma(I)]	R1 = 0.0677, wR2 = 0.1566
R indices (all data)	R1 = 0.0774, wR2 = 0.1624
Largest diff. peak and hole	2.856 and -1.456 e/Å ⁻³

Table 3. Crystal data and structure refinement for **2b**.

Identification code	1850177
Empirical formula	C ₂₅ H ₄₃ BrF ₃ N ₄ PPd
Formula Weight	673.91
Temperature	100.0(3) K
Wavelength	1.54184 Å
Crystal system	Triclinic
Space group	P -1
Unit cell dimensions	a = 9.4690(4) Å $\alpha = 84.683^\circ$ b = 10.4518(5) Å $\beta = 88.622(4)^\circ$ c = 14.1987(8) Å $\gamma = 82.200^\circ$
Volume	1386.13(12) Å ³
Z	2
Density (calculated)	1.615 Mg/m ³
Absorption coefficient	7.985 mm ⁻¹
F(000)	688
Crystal size	0.181 x 0.028 x 0.025 mm ³
Theta range for data collection	3.126 to 63.687°
Index ranges	-11 ≤ h ≤ 11, -12 ≤ k ≤ 12, -16 ≤ l ≤ 14
Reflections collected	16904
Independent reflections	4548 [R(int) = 0.0671]
Completeness to theta = 25.242°	99.8%
Absorption correction	Gaussian
Max. and min. transmission	0.933 and 0.468
Refinement method	Full-matrix least squares on F ²
Data / restraints / parameters	4548 / 0 / 322
Goodness-of-fit on F ²	1.253
Final R indices [I > 2sigma(I)]	R1 = 0.0505, wR2 = 0.1456
R indices (all data)	R1 = 0.0721, wR2 = 0.2271
Largest diff. peak and hole	1.214 and -2.293 e/Å ⁻³

Table 4. Crystal data and structure refinement for **3**.

Identification code	1850179
Empirical formula	C ₄₁ H ₅₂ F ₁₂ N ₅ OPPd
Formula Weight	996.24
Temperature	99.97(10) K
Wavelength	0.71073 Å
Crystal system	Triclinic
Space group	P -1
Unit cell dimensions	a = 11.0795(3) Å α = 94.751(2)° b = 12.40313) Å β = 90.188(2)° c = 16.3436(4) Å γ = 107.535(2)°
Volume	2133.29(10) Å ³
Z	2
Density (calculated)	1.515 Mg/m ³
Absorption coefficient	0.565 mm ⁻¹
F(000)	1020
Crystal size	0.25 x 0.166 x 0.032 mm ³
Theta range for data collection	2.453 to 28.588°
Index ranges	-14 ≤ h ≤ 14, -16 ≤ k ≤ 15, -21 ≤ l ≤ 21
Reflections collected	25434
Independent reflections	9224 [R(int) = 0.0334]
Completeness to theta = 25.242°	99.9%
Absorption correction	Gaussian
Max. and min. transmission	1.000 and 0.652
Refinement method	Full-matrix least squares on F ²
Data / restraints / parameters	9224 / 0 / 557
Goodness-of-fit on F ²	1.047
Final R indices [I > 2σ(I)]	R1 = 0.0358, wR2 = 0.0750
R indices (all data)	R1 = 0.0416, wR2 = 0.0783
Largest diff. peak and hole	1.906 and -0.834 e/Å ⁻³